Inorg. Chem. **2007**, *46*, 11003–11016

cis-Dicyanoosmium(II) Diimine Complexes Bearing Phosphine or Sulfoxide Ligands: Spectroscopic and Luminescent Studies

Siu-Wai Lai,* Queenie K.-W. Chan, Nianyong Zhu, and Chi-Ming Che*

Department of Chemistry and Open Laboratory of Chemical Biology of the Institute of Molecular Technology for Drug Discovery and Synthesis, and HKU-CAS Joint Laboratory on New Materials, The University of Hong Kong, Pokfulam Road, Hong Kong SAR, China

Received February 13, 2007

A series of *cis*-dicyanoosmium(II) complexes $[Os(PPh_3)_2(CN)_2(N^{\cap}N)]$ ($N^{\cap}N$ = Ph_2phen (**2a**), bpy (**2b**), phen (**2c**), Ph_2bpy (**2d**), $^tBu_2$bpy (**2e**)) and $[Os(DMSO)_2(CN)_2(N^{\cap}N)]$ (**3a**-**3e**, $N^{\cap}N$ = Br_2phen (**3f**), Clphen (**3g**)), were synthesized and their spectroscopic and photophysical properties were examined, and $[Os(PMe_3)_2(CN)_2(phen)]$ (**4**) with axial PMe_3 ligands was similarly prepared. The molecular structures of **2a**, **2c**, $[\mathbf{2c}\cdot Zn(NO_3)_2]_\infty$, **2d**, **2e**, **3b**, **3d**, **3e**, and **4** were determined by X-ray crystallographic analyses. The two CN ligands are cis to each other with mean Os–C bond distance of 2.0 Å. The two PR_3 (R = Ph, Me) or DMSO ligands are trans to each other with P/S–Os–P/S angles of ∼177°. The UV–vis absorption spectra of **2a**–**2e** display an intense absorption band at 268–315 nm (ϵ = ∼(1.54–4.82) × 10^4 M^{-1} cm^{-1}) that are attributed to $\pi \rightarrow \pi^*(N^{\cap}N)$ and/or $\pi \rightarrow \pi^*(PPh_3)$ transitions. The moderately intense absorption bands with λ_{max} at 387–460 nm (ϵ = ∼ (2.4–11.3) × 10^3 M^{-1} cm^{-1}) are attributed to a ^{1}MLCT transition. A weak, broad absorption at 487–600 nm (ϵ = ∼390–1900 M^{-1} cm^{-1}) is assigned to a ^{3}MLCT transition. Excitation of **2a**–**2e** in dichloromethane at 420 nm gives an emission with peak maximum at 654–703 nm and lifetime of 0.16–0.67 μs. The emission energies, lifetimes, and quantum yields show solvatochromic responses, and plots of ν_{max}, τ, and Φ, respectively, versus E_T (solvent polarity parameter) show linear correlations, indicating that the emission is sensitive to the local environment. The broad structureless solid-state emission of **2a**–**2e** at 298 (λ_{max} 622–707 nm) and 77 (λ_{max} 602–675 nm) K are assigned to ^{3}MLCT excited states. The 77 K MeOH/EtOH (1:4) glassy solutions of **2a**–**2e** also exhibit ^{3}MLCT emissions with λ_{max} = 560–585 nm. The ^{1}MLCT absorption and ^{3}MLCT emission of **3a**–**3g** occur at λ_{max} = 332–390 nm and 553–644 nm, respectively. In the presence of $Zn(NO_3)_2$, both the ^{1}MLCT absorption and ^{3}MLCT emission of **2c** in acetonitrile blue-shift from 397 to 341 nm and 651 to 531 nm, respectively. The enhancement of emission intensity (I/I_0) of **2e** at 531 nm reached a maximum of ∼810 upon the addition of two equivs of $Zn(NO_3)_2$. The crystallographic and spectroscopic evidence suggests that **2c** undergoes binding of Zn^{2+} ions via the cyano moieties.

Introduction

Transition-metal complexes that display intense phosphorescence from metal-to-ligand charge transfer (MLCT) excited states have been widely investigated,[1] including inter alia for photoinduced electron-transfer reactions[2] and as chemosensory,[3,4] electroluminescent (in organic light-emitting devices),[5,6] and photovoltaic (in solar cells)[7] materials. In

* To whom correspondence should be addressed. Email: cmche@hku.hk (C.-M.C.), swlai@hku.hk (S.-W.L.).

(1) (a) Lehn, J.-M. *Supramolecular Chemistry*; VCH Publishers: Weinheim, Germany, 1995. (b) Fabbrizzi, L.; Licchelli, M.; Pallavicini, P. In *Transition Metals in Supramolecular Chemistry*; Sauvage, J.-P., Ed.; Wiley & Sons: New York, 1999. (c) Sauvage, J.-P.; Collin, J.-P.; Chambron, J.-C.; Guillerez, S.; Coudret, C.; Balzani, V.; Barigelletti, F.; De Cola, L.; Flamigni, L. *Chem. Rev.* **1994**, *94*, 993−1019.

(2) (a) Loiseau, F.; Marzanni, G.; Quici, S.; Indelli, M. T.; Campagna, S. *Chem. Commun.* **2003**, 286−287. (b) Bergamini, G.; Saudan, C.; Ceroni, P.; Maestri, M.; Balzani, V.; Gorka, M.; Lee, S.-K.; van Heyst, J.; Vögtle, F. *J. Am. Chem. Soc.* **2004**, *126*, 16466−16471. (c) Lainé, P. P.; Bedioui, F.; Loiseau, F.; Chiorboli, C.; Campagna, S. *J. Am. Chem. Soc.* **2006**, *128*, 7510−7521.

(3) (a) Beer, P. D.; Szemes, F.; Balzani, V.; Salà, C. M.; Drew, M. G. B.; Dent, S. W.; Maestri, M. *J. Am. Chem. Soc.* **1997**, *119*, 11864−11875. (b) Beer, P. D. *Acc. Chem. Res.* **1998**, *31*, 71−80. (c) Beer, P. D.; Cadman, J. *New J. Chem.* **1999**, *23*, 347−349. (d) Beer, P. D.; Cadman, J. *Coord. Chem. Rev.* **2000**, *205*, 131−155.

(4) (a) Prodi, L.; Bolletta, F.; Montalti, M.; Zaccheroni, N. *Coord. Chem. Rev.* **2000**, *205*, 59−83. (b) Keefe, M. H.; Benkstein, K. D.; Hupp, J. T. *Coord. Chem. Rev.* **2000**, *205*, 201−228. (c) Hu, Y.-Z.; Xiang, Q.; Thummel, R. P. *Inorg. Chem.* **2002**, *41*, 3423−3428.

10.1021/ic070290l CCC: $37.00
Published on Web 11/22/2007

the literature, studies in this area are mainly confined to d^6 metal ions containing polypyridyl ligands,[8,9] which display intense absorption and emission in the visible region. Previous reports have shown that d^6 metal complexes containing cyanide and polypyridyl ligands can noncovalently interact with solvent molecules, and their emission properties are sensitive to the polarity of the local medium.[10−12] The observation of solvatochromic charge-transfer absorption spectra for metal-cyanide complexes such as $[Fe(diimine)_2(CN)_2]$ was first described by Burgess.[13] Subsequently, La Mar and co-workers noted that intermolecular O−H(solvent)···N≡C and C−H···N≡C interactions could affect the electronic properties of dicyano(porphyrinato)-ferrate(III).[14] Furthermore, complexes bearing protonated,[15] metalated,[16,17] and Lewis-acid (BF_3)[18] adducts of cyano ligands with spectral properties that are significantly different from counterparts with free cyano moieties have been reported.

Luminescent osmium(II) complexes are relatively underdeveloped[19−21] when compared to the ruthenium(II) analogues with polypyridyl ligands,[22] yet practical applications can nevertheless be envisaged. For example, it has been reported that luminescent osmium(II) derivatives such as $[Os(diimine)_3]^{2+}$ can potentially function as oxygen sensors,[23] whereas $[Os(N^{\cap}N)_2(L^{\wedge}L)]^{2+}$ ($N^{\cap}N$ = substituted phenanthroline; $L^{\wedge}L$ = strong π-acid ligand, e.g., $Ph_2AsCH{=}CHAsPh_2$ or $Ph_2PCH{=}CHPPh_2$) and $[Os(fptz)_2(PPh_2Me)_2]$ (fptzH = 3-trifluoromethyl-5-(2-pyridyl)-1,2,4-triazole) have been utilized as OLED materials.[24] Here, we report a class of solvatochromic dicyanoosmium(II) complexes containing a variety of diimine ligands. Notably, the water-soluble DMSO-derivatized osmium(II) complexes have been developed, thereby providing an entry to a new family of phosphorescent sensory materials with applications in aqueous medium.

Experimental Section

Synthesis and General Procedures. 4,7-Diphenyl-1,10-phenanthroline (Ph_2phen), 2,2′-bipyridine (bpy), 1,10-phenanthroline (phen), 4,4′-diphenyl-2,2′-bipyridine (Ph_2bpy), 4,4′-di-*tert*-butyl-2,2′-bipyridine ($^tBu_2$bpy), and 5-chloro-1,10-phenanthroline (Clphen) were purchased from Aldrich. Syntheses of 5,6-dibromo-1,10-phenanthroline (Br_2phen),[25] $K_2[Os^{VI}O_2(OH)_4]$,[26] and $[OsO_2(CN)_2(N^{\cap}N)]$ ($N^{\cap}N$ = Ph_2phen,[19,27] bpy,[28] $^tBu_2$bpy)[29] were prepared according to literature procedures. Dichloromethane for photophysical studies was washed with concentrated sulfuric acid, 10% sodium hydrogen carbonate, and water, dried by calcium chloride, and distilled over calcium hydride. Acetonitrile for photophysical measurements was distilled over potassium permanganate and calcium hydride. All of the other solvents were of analytical grade and purified according to conventional methods.[30]

Instrumentation and Physical Measurements. Fast atom bombardment (FAB) mass spectra were obtained on a Finnigan Mat 95 mass spectrometer with a 3-nitrobenzyl alcohol matrix, whereas electrospray mass spectra were obtained on a LCQ quadrupole ion-trap mass spectrometer. ^{1}H (500 MHz), ^{13}C (126

(5) (a) Baldo, M. A.; O'Brien, D. F.; You, Y.; Shoustikov, A.; Sibley, S.; Thompson, M. E.; Forrest, S. R. *Nature* **1998**, *395*, 151−154. (b) Adachi, C.; Baldo, M. A.; Forrest, S. R.; Lamansky, S.; Thompson, M. E.; Kwong, R. C. *Appl. Phys. Lett.* **2001**, *78*, 1622−1624. (c) Ma, Y.; Zhang, H.; Shen, J.; Che, C. *Synth. Met.* **1998**, *94*, 245−248.

(6) (a) Welter, S.; Brunner, K.; Hofstraat, J. W.; De Cola, L. *Nature* **2003**, *421*, 54−57. (b) Kalyuzhny, G.; Buda, M.; McNeill, J.; Barbara, P.; Bard, A. J. *J. Am. Chem. Soc.* **2003**, *125*, 6272−6283. (c) Slinker, J.; Bernards, D.; Houston, P. L.; Abruña, H. D.; Bernhard, S.; Malliaras, G. G. *Chem. Commun.* **2003**, 2392−2399.

(7) (a) Grätzel, M. *Nature* **2001**, *414*, 338−344. (b) Wang, P.; Zakeeruddin, S. M.; Moser, J. E.; Humphry-Baker, R.; Comte, P.; Aranyos, V.; Hagfeldt, A.; Nazeeruddin, M. K.; Grätzel, M. *Adv. Mater.* **2004**, *16*, 1806−1811.

(8) (a) Balzani, V.; Scandola, F. In *Supramolecular Photochemistry*; Ellis Horwood: New York, 1991. (b) Watanabe, S.; Onogawa, O.; Komatsu, Y.; Yoshida, K. *J. Am. Chem. Soc.* **1998**, *120*, 229−230. (c) Mizuno, T.; Wei, W.-H.; Eller, L. R.; Sessler, J. L. *J. Am. Chem. Soc.* **2002**, *124*, 1134−1135. (d) Anzenbacher, Jr. P.; Tyson, D. S.; Jursíková, K.; Castellano, F. N. *J. Am. Chem. Soc.* **2002**, *124*, 6232−6233.

(9) (a) Barigelletti, F.; Flamigni, L.; Calogero, G.; Hammarström, L.; Sauvage, J.-P.; Collin, J.-P. *Chem. Commun.* **1998**, 2333−2334. (b) Rau, S.; Büttner, T.; Temme, C.; Ruben, M.; Görls, H.; Walther, D.; Duati, M.; Fanni, S.; Vos, J. G. *Inorg. Chem.* **2000**, *39*, 1621−1624.

(10) (a) Belser, P.; von Zelewsky, A.; Juris, A.; Barigelletti, F.; Balzani, V. *Gazz. Chim. Ital.* **1985**, *115*, 723−729. (b) Simpson, N. R. M.; Ward, M. D.; Morales, A. F.; Barigelletti, F. *J. Chem. Soc., Dalton Trans.* **2002**, 2449−2454.

(11) Curtis, J. C.; Sullivan, B. P.; Meyer, T. J. *Inorg. Chem.* **1983**, *22*, 224−236.

(12) Benniston, A. C.; Mackie, P. R.; Farrugia, L. J.; Smith, G.; Teat, S. J.; McLean, A. J. *New J. Chem.* **2001**, *25*, 458−464.

(13) (a) Burgess, J. *Spectrochim. Acta* **1970**, *26A*, 1369−1374. (b) Burgess, J. *Spectrochim. Acta* **1970**, *26A*, 1957−1962. (c) Podsiadla, M.; Rzeszotarska, J.; Kalinowski, M. K. *Monatsh. Chem.* **1994**, *125*, 827−831.

(14) (a) Frye, J. S.; La Mar, G. N. *J. Am. Chem. Soc.* **1975**, *97*, 3561−3562. (b) La Mar, G. N.; Gaudio, J. D.; Frye, J. S. *Biochim. Biophys. Acta* **1977**, *498*, 422−435. (c) Ikezaki, A.; Nakamura, M. *Inorg. Chem.* **2002**, *41*, 2761−2768. (d) Ikezaki, A.; Nakamura, M. *Inorg. Chem.* **2003**, *42*, 2301−2310.

(15) (a) Peterson, S. H.; Demas, J. N. *J. Am. Chem. Soc.* **1976**, *98*, 7880−7881. (b) Peterson, S. H.; Demas, J. N. *J. Am. Chem. Soc.* **1979**, *101*, 6571−6577.

(16) Kinnaird, M. G.; Whitten, D. G. *Chem. Phys. Lett.* **1982**, *88*, 275−280.

(17) (a) Demas, J. N.; Addington, J. W. *J. Am. Chem. Soc.* **1974**, *96*, 3663−3664. (b) Demas, J. N.; Addington, J. W.; Peterson, S. H.; Harris, E. W. *J. Phys. Chem.* **1977**, *81*, 1039−1043. (c) Bartocci, C.; Bignozzi, C. A.; Scandola, F.; Rumin, R.; Courtot, P. *Inorg. Chim. Acta* **1983**, *76*, L119−L121. (d) Bignozzi, C. A.; Scandola, F. *Inorg. Chem.* **1984**, *23*, 1540−1545. (e) Bignozzi, C. A.; Roffia, S.; Scandola, F. *J. Am. Chem. Soc.* **1985**, *107*, 1644−1651. (f) Chow, C.-F.; Lam, M. H. W.; Sui, H.; Wong, W.-Y. *Dalton Trans.* **2005**, 475−484.

(18) Shriver, D. F.; Posner, J. *J. Am. Chem. Soc.* **1966**, *88*, 1672−1677.

(19) Cheng, J. Y. K.; Cheung, K.-K.; Che, C.-M. *Chem. Commun.* **1997**, 623−624.

(20) El-ghayoury, A.; Harriman, A.; Ziessel, R. *Chem. Commun.* **1999**, 2027−2028.

(21) Chen, Y.-L.; Lee, S.-W.; Chi, Y.; Hwang, K.-C.; Kumar, S. B.; Hu, Y.-H.; Cheng, Y.-M.; Chou, P.-T.; Peng, S.-M.; Lee, G.-H.; Yeh, S.-J.; Chen, C.-T. *Inorg. Chem.* **2005**, *44*, 4287−4294.

(22) (a) Juris, A.; Balzani, V.; Barigelletti, F.; Campagna, S.; Belser, P.; von Zelewsky, A. *Coord. Chem. Rev.* **1988**, *84*, 85−277 and references therein. (b) Derossi, S.; Adams, H.; Ward, M. D. *Dalton Trans.* **2007**, 33−36.

(23) Xu, W.; Kneas, K. A.; Demas, J. N.; DeGraff, B. A. *Anal. Chem.* **1996**, *68*, 2605−2609.

(24) (a) Carlson, B.; Phelan, G. D.; Kaminsky, W.; Dalton, L.; Jiang, X.; Liu, S.; Jen, A. K.-Y. *J. Am. Chem. Soc.* **2002**, *124*, 14162−14172. (b) Tung, Y.-L.; Lee, S.-W.; Chi, Y.; Tao, Y.-T.; Chien, C.-H.; Cheng, Y.-M.; Chou, P.-T.; Peng, S.-M.; Liu, C.-S. *J. Mater. Chem.* **2005**, *15*, 460−464. (c) Chou, P.-T.; Chi, Y. *Eur. J. Inorg. Chem.* **2006**, 3319−3332.

(25) Feng, M.; Chan, K. S. *Organometallics* **2002**, *21*, 2743−2750.

(26) Malin, J. M. *Inorg. Synth.* **1980**, *20*, 61−63.

(27) Cheng, J. Y. K.; Cheung, K.-K.; Che, C.-M.; Lau, T.-C. *Chem. Commun.* **1997**, 1443−1444.

(28) Sartori, C.; Preetz, W. *Z. Anorg. Allg. Chem.* **1989**, *572*, 151−163.

(29) Chin, K.-F.; Cheng, Y.-K.; Cheung, K.-K.; Guo, C.-X.; Che, C.-M. *J. Chem. Soc., Dalton Trans.* **1995**, 2967−2973.

(30) Perrin, D. D.; Armarego, W. L. F.; Perrin, D. R. *Purification of Laboratory Chemicals*, 2nd ed.; Pergamon Press: Oxford, U.K., 1980.

MHz), and ^{31}P (202 MHz) NMR measurements were performed on a DPX 500 Bruker FT-NMR spectrometer with chemical shifts (in ppm) relative to tetramethylsilane (^{1}H and ^{13}C) and H_3PO_4 (^{31}P) as references. Elemental analyses were performed by the Institute of Chemistry at the Chinese Academy of Sciences, Beijing. Infrared spectra were recorded on a Bio-Rad FTIR spectrophotometer. UV−vis spectra were recorded on a PerkinElmer Lambda 19 UV/vis spectrophotometer. Thermal analyses were performed on a PerkinElmer TGA 7 thermogravimetric analyzer (heating rate = 15 °C/min, N_2 atmosphere). Cyclic voltammetry was performed using a Bioanalytical Systems model 100 B/W electrochemical analyzer. The electrochemical cell was a conventional two-compartment cell with a glassy carbon disk as the working electrode, an $Ag|AgNO_3$ (0.1 M) electrode as the reference electrode, and a platinum wire as the counter electrode. Tetrabutylammonium hexafluorophosphate (0.1 M) was used as the supporting electrolyte. The ferrocenium/ferrocene was used as internal reference and all of the potentials were quoted with respect to $Cp_2Fe^{+/0}$. The $E_{1/2}$ values were taken as the average of the cathodic and anionic peak potentials for the oxidative and reductive waves.

Emission and Lifetime Measurements. Steady-state emission spectra were recorded on a Fluorolog-3 Model FL3−21 spectrophotometer. Solution samples for measurements were degassed with at least four freeze−pump−thaw cycles. Low-temperature (77 K) emission spectra for glassy solutions and solid-state samples were recorded in 5 mm diameter quartz tubes, which were placed in a liquid nitrogen Dewar flask equipped with quartz windows. The emission spectra were corrected for monochromator and photomultiplier efficiency and for xenon lamp stability. Emission lifetime measurements were performed with a Quanta Ray DCR-3 pulsed Nd:YAG laser system (pulse output 355 nm, 8 ns). Errors for λ values (±1 nm), τ (±10%), Φ (±10%) were estimated.

Luminescence quantum yields were determined using the method of Demas and Crosby[31] with $[Ru(bpy)_3]Cl_2$ in degassed acetonitrile as a standard reference solution ($\Phi_r = 0.062$) and calculated according to the following equation: $\Phi_s = \Phi_r(B_r/B_s)(n_s/n_r)^2(D_s/D_r)$, where the subscripts s and r refer to sample and reference standard solution respectively, n is the refractive index of the solvents, D is the integrated intensity, and Φ is the luminescence quantum yield. The quantity B was calculated by $B = 1 - 10^{-AL}$, where A is the absorbance at the excitation wavelength and L is the optical path length. The radiative (k_r) and nonradiative (k_{nr}) rate constants were calculated by $k_r = \Phi_0/\tau_0$ and $k_{nr} = k_r(1/\Phi_0 - 1)$, respectively. Solid-state emission quantum yields were determined by the method of Wrighton et al.,[32] using KBr as the standard, and calculated by $\Phi = E/(R_{std} - R_{smpl})$, where E is the area under the corrected emission curve of the sample, and R_{std} and R_{smpl} are the corrected areas under the diffuse reflectance curves of the nonabsorbing standard and the sample, respectively, at the excitation wavelength.

$[OsO_2(CN)_2(N^\frown N)]$ ($N^\frown N$ = Ph$_2$phen (1a), bpy (1b), phen (1c), Ph$_2$bpy (1d), ^{t}Bu$_2$bpy (1e), Br$_2$phen (1f), Clphen (1g)). $K_2[Os^{VI}O_2(CN)_2(OH)_2]$ was prepared by literature method.[19] Previous reports revealed that *cis*-dicyano dioxoosmium(VI) diimine complexes for $N^\frown N$ = Ph$_2$phen (**1a**),[19,27] bpy (**1b**),[28] and ^{t}Bu$_2$bpy (**1e**)[29] were prepared by the addition of a $N^\frown N$ ligand in dichloromethane to a freshly prepared aqueous solution of $K_2[Os^{VI}O_2(CN)_2(OH)_2]$, in the presence of tetrabutylammonium chloride and acetic acid at room temperature. Similarly, **1c**, **1d**, **1f**, and **1g** were prepared according to literature procedures.[19,27−29]

(31) Demas, J. N.; Crosby, G. A. *J. Phys. Chem.* **1971**, *75*, 991−1024.
(32) Wrighton, M. S.; Ginley, D. S.; Morse, D. L. *J. Phys. Chem.* **1974**, *78*, 2229−2233.

$[OsO_2(CN)_2(phen)]$, 1c. Yield: 0.17 g, 72%. ^{1}H NMR (DMSO-d_6): δ 8.47−8.50 (m, 2H), 8.55 (s, 2H), 9.34 (dd, J = 8.3, 1.2 Hz, 2H), 9.99 (dd, J = 5.1, 1.2 Hz, 2H). FAB-MS: m/z 457 $[M + H]^+$, 443 $[M + H-N]^+$, 430 $[M-CN]^+$, 414 $[M-CN-O]^+$, 404 $[M-2CN]^+$. Anal. Calcd for $C_{14}H_8N_4O_2Os$: C, 37.00; H, 1.77; N, 12.33. Found: C, 36.92; H, 1.90; N, 12.57. IR (KBr): ν 2157 (C≡N), 861 (Os═O) cm^{-1}.

$[OsO_2(CN)_2(Ph_2bpy)]$, 1d. Yield: 0.27 g, 89%. ^{1}H NMR (DMSO-d_6): δ 7.69−7.71 (m, 6H), 8.18−8.21 (m, 4H), 8.50 (d, J = 6.0 Hz, 2H), 9.51 (s, 2H), 9.65 (d, J = 5.9 Hz, 2H). FAB-MS: m/z 585 $[M + H]^+$, 569 $[M + H-O]^+$, 558 $[M-CN]^+$, 542 $[M-CN-O]^+$. Anal. Calcd for $C_{24}H_{16}N_4O_2Os$: C, 49.48; H, 2.77; N, 9.62. Found: C, 49.10; H, 2.87; N, 9.24. IR (KBr): ν 2162 (C≡N), 851 (Os═O) cm^{-1}.

$[OsO_2(CN)_2(Br_2phen)]$, 1f. Yield: 0.12 g, 38%. ^{1}H NMR (DMSO-d_6): δ 8.54−8.57 (m, 2H), 9.45 (d, J = 8.2 Hz, 2H), 10.04 (d, J = 4.4 Hz, 2H). FAB-MS: m/z 613 $[M + H]^+$, 597 $[M + H-O]^+$, 581 $[M + H-2O]^+$. Anal. Calcd for $C_{14}H_6N_4Br_2O_2Os$: C, 27.47; H, 0.99; N, 9.15. Found: C, 27.22; H, 1.13; N, 8.87. IR (KBr): ν 2157 (C≡N), 860 (Os═O) cm^{-1}.

$[OsO_2(CN)_2(Clphen)]$, 1g. Yield: 0.13 g, 51%. ^{1}H NMR (DMSO-d_6): δ 8.49−8.58 (m, 2H), 8.87 (s, 1H), 9.25 (d, J = 8.2 Hz, 1H), 9.43 (d, J = 8.8 Hz, 1H), 9.97 (d, J = 4.8 Hz, 1H), 10.07 (d, J = 4.6 Hz, 1H). FAB-MS: m/z 491 $[M + H]^+$, 476 $[M + 2H - O]^+$, 461 $[M + 3H - 2O]^+$. Anal. Calcd for $C_{14}H_7N_4ClO_2Os$: C, 34.40; H, 1.44; N, 11.46. Found: C, 34.28; H, 1.55; N, 11.67. IR (KBr): ν 2159 (C≡N), 853 (Os═O) cm^{-1}.

$[Os(PPh_3)_2(CN)_2(N^\frown N)]$ ($N^\frown N$ = Ph$_2$phen (2a), bpy (2b), phen (2c), Ph$_2$bpy (2d), ^{t}Bu$_2$bpy (2e)). To a stirred solution of $[OsO_2(CN)_2(N^\frown N)]$ (0.95 mmol) in dichloromethane (15 mL) was added a solution of PPh_3 (1.5 g, 5.73 mmol) in methanol (15 mL). The mixture was transferred to a quartz tube, stirred, and exposed to broad-band irradiation (λ > 290 nm) with a 400 W mercury arc lamp under a nitrogen atmosphere for 4 h. The solvent was removed under vacuum to give a brown solid. The crude product was purified by chromatography on a silica gel column using dichloromethane to remove excess PPh_3 and the dioxoosmium(VI) precursor, and the orange product was eluted with CH_2Cl_2/CH_3OH (4:1 v/v) mixture. Removal of the solvent under vacuum gave a deep-red solid, which was recrystallized to give dark-red or brown crystals by diffusion of diethyl ether into a dichloromethane solution. Synthesis and characterization of **2a** were reported previously.[19]

$[Os(PPh_3)_2(CN)_2(bpy)]$, 2b. Yield: 0.64 g, 73%. ^{1}H NMR (CD_3OD): δ 6.63 (t, J = 7.0 Hz, 2H), 7.16−7.28 (m, 18H, PPh_3), 7.45−7.51 (m, 12H, PPh_3), 7.63 (t, J = 7.6 Hz, 2H), 8.15 (d, J = 8.2 Hz, 2H), 8.31 (d, J = 5.8 Hz, 2H). ^{13}C{^{1}H} NMR ($CDCl_3$/CD_3OD 15:1 v/v): δ 120.8, 127.0, 127.8 (t, J = 4.7 Hz), 129.2, 131.6 (t, J = 23.9 Hz), 133.6 (t, J = 5.1 Hz), 134.0, 154.0, 156.4, Os−*C*N not resolved. ^{31}P{^{1}H} NMR ($CDCl_3/CD_3OD$ 15:1 v/v): δ 4.53. FAB-MS: m/z 925 $[M + H]^+$, 636 $[M- PPh_3-CN]^+$. Anal. Calcd for $C_{48}H_{38}N_4P_2Os$: C, 62.46; H, 4.15; N, 6.07. Found: C, 62.33; H, 4.03; N, 6.01. IR (KBr): ν 2048, 2070 (C≡N) cm^{-1}.

$[Os(PPh_3)_2(CN)_2(phen)]$, 2c. Yield: 0.56 g, 62%. ^{1}H NMR ($CDCl_3$): δ 6.82 (dd, J = 8.1, 5.3 Hz, 2H), 7.03−7.13 (m, 18H, PPh_3), 7.26−7.33 (m, 12H, PPh_3), 7.77 (s, 2H), 7.87 (d, J = 8.0 Hz, 2H), 8.90 (d, J = 5.3 Hz, 2H). ^{13}C{^{1}H} NMR ($CDCl_3$): δ 125.5, 126.7, 127.7 (t, J = 4.7 Hz), 128.9, 129.1, 131.6 (t, J = 23.8 Hz), 132.6, 133.6 (t, J = 5.1 Hz), 148.3, 154.5, Os−*C*N not resolved. ^{31}P{^{1}H} NMR ($CDCl_3$): δ 4.77. FAB-MS: m/z 949 $[M + H]^+$, 660 $[M-PPh_3-CN]^+$. Anal. Calcd for $C_{50}H_{38}N_4P_2Os$: C, 63.41; H, 4.04; N, 5.92. Found: C, 63.48; H, 3.91; N, 5.91. IR (KBr): ν 2053, 2068 (C≡N) cm^{-1}.

[Os(PPh$_3$)$_2$(CN)$_2$(Ph$_2$bpy)], 2d. Yield: 0.66 g, 65%. ^{1}H NMR ($CDCl_3$): δ 6.62 (d, J = 6.0 Hz, 2H), 7.13−7.14 (m, 18H, PPh_3), 7.53−7.57 (m, 22H, PPh_3 and Ph), 7.92 (s, 2H), 8.64 (d, J = 6.1 Hz, 2H). ^{13}C{^{1}H} NMR ($CDCl_3$): δ 118.7, 124.7, 126.8, 127.7 (t, J = 4.7 Hz), 128.9, 129.5, 129.8, 132.1 (t, J = 23.6 Hz), 133.8 (t, J = 5.2 Hz), 136.9, 146.6, 154.2, 157.0, Os−*C*N not resolved. ^{31}P{^{1}H} NMR ($CDCl_3$): δ 3.63. FAB-MS: *m*/*z* 1075 [M−H]$^+$, 998 [M−Ph−H]$^+$, 814 [M−PPh_3]$^+$, 787 [M−PPh_3−CN−H]$^+$. Anal. Calcd for $C_{60}H_{46}N_4P_2Os$: C, 67.03; H, 4.31; N, 5.21. Found: C, 66.65; H, 4.30; N, 5.02. IR (KBr): ν 2052, 2072 (C≡N) cm^{-1}.

[Os(PPh$_3$)$_2$(CN)$_2$(^{t}Bu$_2$bpy)], 2e. Yield: 0.69 g, 70%. ^{1}H NMR ($CDCl_3$): δ 1.28 (s, 18H, ^{t}Bu), 6.40 (dd, J = 6.1, 2.0 Hz, 2H), 7.08−7.14 (m, 18H, PPh_3), 7.44−7.48 (m, 12H, PPh_3), 7.58 (d, J = 1.9 Hz, 2H), 8.39 (d, J = 6.1 Hz, 2H). ^{13}C{^{1}H} NMR ($CDCl_3$): δ 30.6 (C*Me$_3$*), 34.8 (*C*Me$_3$), 116.6, 124.3, 127.6 (t, J = 4.6 Hz), 128.7, 132.2 (t, J = 23.5 Hz), 133.8 (t, J = 5.2 Hz), 153.5, 156.4, 158.6, Os−*C*N not resolved. ^{31}P{^{1}H} NMR ($CDCl_3$): δ 4.74. FAB-MS: *m*/*z* 1035 [M−H]$^+$, 959 [M−Ph]$^+$, 774 [M−PPh_3]$^+$, 747 [M−PPh_3−CN−H]$^+$, 719 [M−PPh_3−2CN−3H]$^+$. Anal. Calcd for $C_{56}H_{54}N_4P_2Os$: C, 64.97; H, 5.26; N, 5.41. Found: C, 64.59; H, 5.60; N, 5.15. IR (KBr): ν 2055, 2074 (C≡N) cm^{-1}.

[Os(DMSO)$_2$(CN)$_2$(N^N)] (N^N = Ph$_2$phen (3a), bpy (3b), phen (3c), Ph$_2$bpy (3d), ^{t}Bu$_2$bpy (3e), Br$_2$phen (3f), Clphen (3g)). A suspension mixture of [$OsO_2(CN)_2$(N^N)] (0.95 mmol) in dimethyl sulfoxide (30 mL) was transferred to a quartz tube, stirred, and exposed to broad-band irradiation (λ > 290 nm) with a 400 W mercury arc lamp under nitrogen atmosphere for 4 h. The solvent was removed under vacuum to give a brown solid, which was purified by chromatography on a silica gel column, using CH_2Cl_2 to remove SO_2Me_2. The orange product was eluted with CH_2Cl_2/CH_3OH (4:1 v/v) mixture, and recrystallization by diffusion of diethyl ether into a dichloromethane solution gave dark-red or brown crystals. Syntheses and characterization of **3a** were reported previously.[19]

[Os(DMSO)$_2$(CN)$_2$(bpy)], 3b. Yield: 0.27 g, 51%. ^{1}H NMR ($CDCl_3$): δ 3.34 (s, 12H, $SOMe_2$), 7.59 (t, J = 6.6 Hz, 2H), 8.04 (t, J = 7.9 Hz, 2H), 8.15 (d, J = 8.1 Hz, 2H), 9.74 (d, J = 5.6 Hz, 2H). ^{13}C{^{1}H} NMR ($CDCl_3$): δ 46.6 ($SOMe_2$), 122.9, 127.6, 128.8 (C≡N), 137.9, 154.6, 158.8. FAB-MS: *m*/*z* 557 [M + H]$^+$, 479 [M + H− $SOMe_2$]$^+$, 417 [M + 2H − $SOMe_2$− SOMe]$^+$. Anal. Calcd for $C_{16}H_{20}N_4S_2O_2Os$: C, 34.65; H, 3.63; N, 10.10. Found: C, 33.32; H, 3.60; N, 9.99. IR (KBr): ν 2059, 2083 (C≡N) cm^{-1}.

[Os(DMSO)$_2$(CN)$_2$(phen)], 3c. Yield: 0.31 g, 56%. ^{1}H NMR (CD_3OD): δ 3.23 (s, 12H, $SOMe_2$), 8.07−8.11 (dd, J = 8.2, 5.2 Hz, 2H), 8.23 (s, 2H), 8.80−8.82 (dd, J = 8.3, 1.4 Hz, 2H), 9.74−9.76 (dd, J = 5.2, 1.4 Hz, 2H). ^{13}C{^{1}H} NMR ($CDCl_3$): δ 46.5 ($SOMe_2$), 126.1, 127.8, 128.4 (C≡N), 130.7, 137.3, 150.0, 154.7. FAB-MS: *m*/*z* 581 [M + H]$^+$, 518 [M + H−SOMe]$^+$, 503 [M + H−$SOMe_2$]$^+$. Anal. Calcd for $C_{18}H_{20}N_4S_2O_2Os$: C, 37.36; H, 3.48; N, 9.68. Found: C, 37.40; H, 3.55; N, 9.58. IR (KBr): ν 2060, 2091 (C≡N) cm^{-1}.

[Os(DMSO)$_2$(CN)$_2$(Ph$_2$bpy)], 3d. Yield: 0.32 g, 48%. ^{1}H NMR ($CDCl_3$): δ 3.41 (s, 12H, $SOMe_2$), 7.58−7.60 (m, 6H), 7.74−7.76 (m, 6H), 8.34 (d, J = 1.7 Hz, 2H), 9.74 (d, J = 5.9 Hz, 2H). ^{13}C{^{1}H} NMR ($CDCl_3$): δ 46.7 ($SOMe_2$), 120.9, 125.4, 127.3, 129.0 (C≡N), 129.7, 130.7, 136.0, 150.8, 154.5, 159.1. FAB-MS: *m*/*z* 709 [M + H]$^+$, 646 [M + H−SOMe]$^+$, 631 [M + H−$SOMe_2$]$^+$, 568 [M + H−$SOMe_2$− SOMe]$^+$, 542 [M + H−$SOMe_2$−SOMe−CN]$^+$. Anal. Calcd for $C_{28}H_{28}N_4S_2O_2Os$: C, 47.58; H, 3.99; N, 7.93. Found: C, 47.43; H, 4.02; N, 7.81. IR (KBr): ν 2068, 2089 (C≡N) cm^{-1}.

[Os(DMSO)$_2$(CN)$_2$(^{t}Bu$_2$bpy)], 3e. Yield: 0.34 g, 54%. ^{1}H NMR ($CDCl_3$): δ 1.45 (s, 18H, ^{t}Bu), 3.36 (s, 12H, $SOMe_2$), 7.53 (dd, J = 6.0, 1.9 Hz, 2H), 8.05 (d, J = 1.9 Hz, 2H), 9.56 (d, J = 5.9 Hz, 2H). ^{13}C{^{1}H} NMR ($CDCl_3$): δ 30.4 (C*Me$_3$*), 35.6 (*C*Me$_3$), 46.6 ($SOMe_2$), 119.8, 124.7, 129.2 (C≡N), 153.9, 158.5, 162.9. FAB-MS: *m*/*z* 669 [M + H]$^+$, 591 [M + H−$SOMe_2$]$^+$, 528 [M + H−$SOMe_2$−SOMe]$^+$, 502 [M + H−$SOMe_2$−SOMe−CN]$^+$. Anal. Calcd for $C_{24}H_{36}N_4S_2O_2Os$: C, 43.22; H, 5.44; N, 8.40. Found: C, 43.05; H, 5.64; N, 8.15. IR (KBr): ν 2064, 2087 (C≡N) cm^{-1}.

[Os(DMSO)$_2$(CN)$_2$(Br$_2$phen)], 3f. Yield: 0.33 g, 50%. ^{1}H NMR ($CDCl_3$): δ 3.32 (s, 12H, $SOMe_2$), 7.99 (dd, J = 8.5, 5.2 Hz, 2H), 8.94 (dd, J = 8.5, 1.3 Hz, 2H), 10.04 (dd, J = 5.2, 1.3 Hz, 2H). ^{13}C{^{1}H} NMR ($CDCl_3$): δ 46.5 ($SOMe_2$), 126.5, 127.4, 127.8 (C≡N), 130.8, 138.5, 149.8, 155.3. FAB-MS: *m*/*z* 739 [M + H]$^+$, 659 [M + H−$SOMe_2$]$^+$, 596 [M + H−$SOMe_2$−SOMe]$^+$, 570 [M + H−$SOMe_2$−SOMe−CN]$^+$. Anal. Calcd for $C_{18}H_{18}N_4S_2O_2Br_2Os$: C, 29.36; H, 2.46; N, 7.61. Found: C, 28.95; H, 2.58; N, 7.47. IR (KBr): ν 2076, 2090 (C≡N) cm^{-1}.

[Os(DMSO)$_2$(CN)$_2$(Clphen)], 3g. Yield: 0.31 g, 56%. ^{1}H NMR ($CDCl_3$): δ 3.30 (s, 6H, $SOMe_2$), 3.33 (s, 6H, $SOMe_2$), 7.93 (dd, J = 8.2, 5.2 Hz, 1H), 8.02 (dd, J = 8.4, 5.2 Hz, 1H), 8.15 (s, 1H), 8.43 (dd, J = 8.3, 1.3 Hz, 1H), 8.88 (dd, J = 8.5, 1.3 Hz, 1H), 9.97 (dd, J = 5.2, 1.3 Hz, 1H), 10.06 (dd, J = 5.2, 1.3 Hz, 1H). ^{13}C{^{1}H} NMR ($CDCl_3$): δ 46.4, 46.5 ($SOMe_2$), 126.4, 126.6, 126.7, 127.9 (C≡N), 128.0 (C≡N), 129.3, 129.8, 132.3, 134.9, 136.4, 149.2, 150.6, 154.7, 155.4. FAB-MS: *m*/*z* 615 [M + H]$^+$, 537 [M + H− $SOMe_2$]$^+$, 475 [M + 2H − $SOMe_2$−SOMe]$^+$, 448 [M + H−$SOMe_2$−SOMe−CN]$^+$. Anal. Calcd for $C_{18}H_{19}N_4S_2O_2ClOs$: C, 35.26; H, 3.12; N, 9.14. Found: C, 35.28; H, 3.45; N, 8.81. IR (KBr): ν 2070, 2089 (C≡N) cm^{-1}.

[Os(PMe$_3$)$_2$(CN)$_2$(phen)], 4. Yield: 0.35 g, 68%. ^{1}H NMR ($CDCl_3$): δ 1.02−1.04 (m, 18H, Me), 7.75 (dd, J = 8.1, 5.3 Hz, 2H), 7.98 (s, 2H), 8.32 (d, J = 8.1 Hz, 2H), 10.13 (d, J = 4.5 Hz, 2H). ^{13}C{^{1}H} NMR ($CDCl_3$): δ 13.2 (t, J = 16.3 Hz, Me), 125.5, 127.5, 130.4, 133.6, 149.2, 154.0, Os−*C*N not resolved. ^{31}P{^{1}H} NMR ($CDCl_3$): δ −38.35. FAB-MS: *m*/*z* 578 [M + 2H]$^+$, 501 [M + H− PMe_3]$^+$. Anal. Calcd for $C_{20}H_{26}N_4P_2Os$: C, 41.81; H, 4.56; N, 9.75. Found: C, 41.51; H, 4.69; N, 9.79. IR (KBr): ν 2025, 2059 (C≡N) cm^{-1}.

X-ray Crystallography. Crystals of **2a**·3CH_2Cl_2, **2c**·2CH_2Cl_2, [**2c**·$Zn(NO_3)_2$]$_\infty$, **2d**·CH_2Cl_2·CH_3CN, **2e**·CH_2Cl_2·H_2O, **3d**·0.5(CH_2Cl_2), **3e**·0.5(CH_2Cl_2)·0.5(Et_2O), and **4**·CH_2Cl_2·2H_2O were obtained by slow diffusion of diethyl ether into dichloromethane solutions, whereas that of **3b**·CH_3OH was obtained by diffusion of diethyl ether into a CH_2Cl_2/CH_3OH (3:1) solution. The crystal data and details of data collection and refinement are summarized in Table 1 and Table S1 in the Supporting Information. The crystal structure of **3a** had previously been reported.[19]

Diffraction data for **2a**·3CH_2Cl_2, **2c**·2CH_2Cl_2, [**2c**·$Zn(NO_3)_2$]$_\infty$, **2d**·CH_2Cl_2·CH_3CN, **2e**·CH_2Cl_2·H_2O, **3b**·CH_3OH, **3d**·0.5(CH_2Cl_2), and **3e**·0.5(CH_2Cl_2)·0.5(Et_2O) were collected on a MAR diffractometer with graphite monochromatized Mo Kα radiation (λ = 0.71073 Å), whereas that of **4**·CH_2Cl_2·2H_2O was collected on a Bruker Smart 1000 CCD diffractometer. The images were interpreted and intensities integrated using the program *DENZO*.[33] The structure was solved by direct method employing *SHELXS-97*[34] (**2e**·CH_2Cl_2·H_2O, **3d**·0.5(CH_2Cl_2), **3e**·0.5(CH_2Cl_2)·0.5(Et_2O), and

(33) Otwinowski, Z.; Minor, W. In *Processing of X-ray Diffraction Data Collected in Oscillation Mode*; Methods in Enzymology, Vol. 276, Macromolecular Crystallography, part A, Carter, C. W., Jr.; Sweet, R. M. Eds.; Academic Press: New York, 1997; pp 307−326.
(34) Sheldrick, G. M. *SHELX 97, Programs for Crystal Structure Analysis*; University of Göttingen: Göttingen, Germany, 1997.

Table 1. Crystal Data

	[**2c**·Zn(NO$_3$)$_2$]$_\infty$	**2d**·CH$_2$Cl$_2$·CH$_3$CN	**3b**·CH$_3$OH	**4**·CH$_2$Cl$_2$·2H$_2$O
formula	$[C_{50}H_{38}N_6O_6OsP_2Zn]_\infty$	$C_{63}H_{51}Cl_2N_5OsP_2$	$C_{17}H_{24}N_4O_3OsS_2$	$C_{21}H_{32}N_4O_2OsP_2Cl_2$
fw	1136.37	1201.13	586.72	695.55
cryst size (mm^3)	0.40 × 0.20 × 0.10	0.35 × 0.35 × 0.20	0.60 × 0.25 × 0.15	0.50 × 0.40 × 0.30
cryst syst	orthorhombic	triclinic	triclinic	monoclinic
space group	*Pnna*	$P\bar{1}$	$P\bar{1}$	*P2/n*
a (Å)	25.929(5)	12.015(2)	7.671(2)	10.882(3)
b (Å)	14.953(3)	13.223(3)	9.465(2)	10.392(3)
c (Å)	11.856(2)	17.861(4)	15.651(3)	12.466(4)
α (deg)	90	83.28(3)	102.86(3)	90
β (deg)	90	87.84(3)	98.04(3)	100.07(2)
γ (deg)	90	75.57(3)	104.78(3)	90
V (Å^3)	4596.8(16)	2729.1(9)	1047.6(4)	1388.0(7)
Z	4	2	2	2
D_c (g cm^{-3})	1.642	1.462	1.860	1.664
μ (cm^{-1})	34.10	25.38	63.10	49.25
$2\theta_{max}$ (deg)	51.32	50.92	50.96	51.34
no. unique data	4304	9415	3523	2636
no. obsd. Data ($I \geq 2\sigma(I)$)	2978	8417	3036	2111
no. variables	295	651	234	149
R[a], R$_w$[b]	0.034, 0.105	0.032, 0.086	0.034, 0.086	0.024, 0.065
residual ρ, eÅ^{-3}	+0.74, −0.79	+0.81, −1.42	+1.76, −2.56	+0.44, −1.20

[a] $R = \sum||F_o| - |F_c||/\sum|F_o|$. [b] $R_w = [\sum w(|F_o| - |F_c|)^2/\sum w|F_o|^2]^{1/2}$.

4·CH$_2$Cl$_2$·2H$_2$O) or *SIR97*[35] program (**2a**·3CH$_2$Cl$_2$, **2c**·2CH$_2$Cl$_2$, [**2c**·Zn(NO$_3$)$_2$]$_\infty$, **2d**·CH$_2$Cl$_2$·CH$_3$CN, and **3b**·CH$_3$OH) on a PC.

For [**2c**·Zn(NO$_3$)$_2$]$_\infty$, the two coordinated NO$_3^-$ are disordered into two sets of positions, each with half occupancy. One crystallographic asymmetric unit consists of half of one formula unit, which is the basic unit of a polymer. The atoms of the disordered NO$_3^-$ ligands were refined isotropically, the other non-hydrogen atoms were refined anisotropically. For **2a**·3CH$_2$Cl$_2$, one crystallographic asymmetric unit consists of one formula unit, including three CH$_2$Cl$_2$ solvent molecules. For **2c**·2CH$_2$Cl$_2$, one crystallographic asymmetric unit consists of half of a formula unit, including one CH$_2$Cl$_2$ solvent molecule. For **2d**·CH$_2$Cl$_2$·CH$_3$CN, one crystallographic asymmetric unit consists of one formula unit, including one dichloromethane and one acetonitrile solvent molecule, which was disordered into two sets of positions. For **2e**·CH$_2$Cl$_2$·H$_2$O, one dichloromethane and one water molecule were also located. One crystallographic asymmetric unit consists of one formula unit.

For **3b**·CH$_3$OH, one crystallographic asymmetric unit consists of one formula unit, including one methanol solvent molecule. For **3d**·0.5(CH$_2$Cl$_2$), one crystallographic asymmetric unit consists of one formula unit, including half of one dichloromethane solvent molecule. For **3e**·0.5(CH$_2$Cl$_2$)·0.5(Et$_2$O), two formula units are in the crystallographic asymmetric unit, including two independent osmium complexes, and one dichloromethane and one diethyl ether molecule. The Platon-squeeze method[36] was used to subtract the effect of unlocated solvent molecules. For **4**·CH$_2$Cl$_2$·2H$_2$O, one crystallographic asymmetric unit consists of half of formula unit, including half of dichloromethane and one water molecule.

Results

Synthesis and Characterization. The synthesis of [OsO$_2$(CN)$_2$(N∩N)] (N∩N = Me$_2$bpy,[29] Ph$_2$phen (**1a**)[19,27] and ^{t}Bu$_2$bpy (**1e**))[29] and [OsL$_2$(CN)$_2$(Ph$_2$phen)] (L = PPh$_3$ (**2a**) and DMSO (**3a**))[19] have previously been communicated. The

Scheme 1

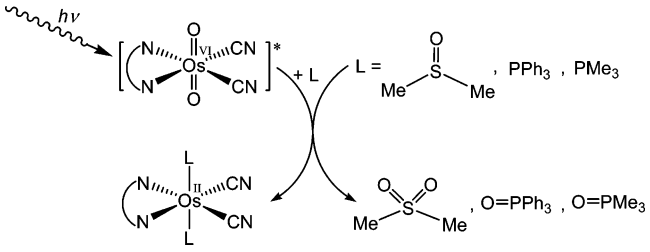

complexes [OsO$_2$(CN)$_2$(N∩N)] (N∩N = bpy (**1b**), phen (**1c**), Ph$_2$bpy (**1d**), Br$_2$phen (**1f**), Clphen (**1g**)) were prepared by the reaction of (^{n}Bu$_4$N)$_2$[OsO$_2$(CN)$_2$(OH)$_2$] with N∩N ligands in dichloromethane in the presence of acetic acid (the crystal structure of **1a** has been reported).[27] Irradiation of a CH$_2$Cl$_2$/CH$_3$OH mixture (1:1 v/v) of [OsO$_2$(CN)$_2$(N∩N)] and PPh$_3$ (6 equiv) using a 400 W mercury arc lamp (λ > 290 nm) for 4 h gave [Os(PPh$_3$)$_2$(CN)$_2$(N∩N)] (N∩N = Ph$_2$phen (**2a**), bpy (**2b**), phen (**2c**), Ph$_2$bpy (**2d**), ^{t}Bu$_2$bpy (**2e**)). The crude products in each case were purified by chromatography on a silica gel column, using CH$_2$Cl$_2$ as eluent to remove greenish-yellow impurities, followed by a CH$_2$Cl$_2$/CH$_3$OH (4:1 v/v) mixture, to elute the product as an orange band. Recrystallization by diffusion of diethyl ether into dichloromethane (with the exception of **2b**) or dichloromethane with 10% methanol (**2b**) solutions yielded brown crystalline solids. Similarly, [Os(PMe$_3$)$_2$(CN)$_2$(phen)] (**4**) was prepared from [OsO$_2$(CN)$_2$(phen)] and PMe$_3$ in 68% yield (Scheme 1).

The complexes [Os(DMSO)$_2$(CN)$_2$(N∩N)] (N∩N = Ph$_2$phen (**3a**), bpy (**3b**), phen (**3c**), Ph$_2$bpy (**3d**), ^{t}Bu$_2$bpy (**3e**), Br$_2$phen (**3f**), Clphen (**3g**)) were obtained by the photolysis of **1a**−**1g** in degassed DMSO for 6 h. The above purification procedure was followed to afford brown crystals of **3a**−**3g** in 50−60% yields. Scheme 2 depicts the molecular structures of **2a**−**2e**, **3a**−**3g**, and **4**. The absorption spectral traces of **1e** (3.91 × 10^{-5} M) in DMSO solution versus time of irradiation using a 400 W mercury arc lamp were recorded: at 0 min, **1e** in DMSO shows a band with λ_{max} at 300−320

(35) Altomare, A.; Burla, M. C.; Camalli, M.; Cascarano, M.; Giacovazzo, C.; Guagliardi, A.; Moliterni, A. G. G.; Polidori, G.; Spagna, R. *SIR97*; *J. Appl. Crystallogr.* **1998**, *32*, 115.
(36) Spek, A. L. *J. Appl. Crystallogr.* **2003**, *36*, 7−13.

Scheme 2. *cis*-Dicyanoosmium(II) Diimine Complexes **2a**−**2e**, **3a**−**3g**, and **4**

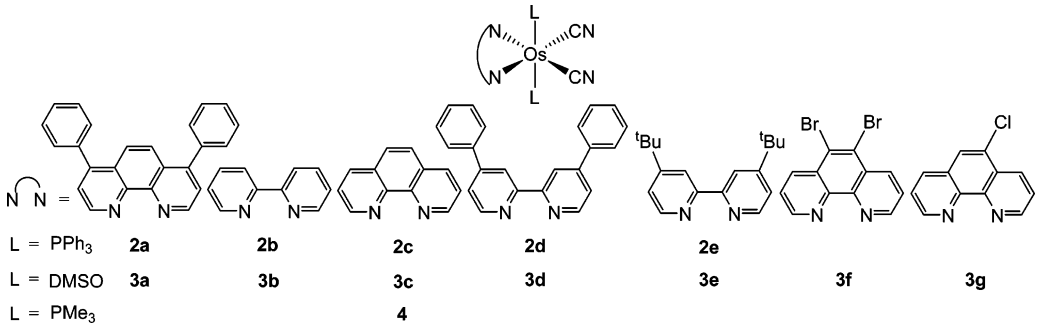

nm; after 1 min, the λ_{max} shifted to ∼288 nm with a broad and intense absorption tailing from 350 to 450 nm, similar to the UV−vis absorption spectrum of **3e** (below), and no isosbestic spectral changes were observed. After photolysis for 6 h, column chromatography of the reaction mixture with dichloromethane as eluent gave dimethyl sulfone (SO_2Me_2),[37] which was characterized by ^{1}H and ^{13}C NMR (δ 2.99 and δ 41.7 respectively in $CDCl_3$) and IR spectroscopy (ν(S═O) 1336 cm^{-1} in KBr). The yield of SO_2Me_2 (based on the dioxo precursor), as analyzed by capillary gas chromatography, was in slight excess of 100%, presumably because of the presence of residual oxygen in the reaction atmosphere.

2a−**2e** and **3a**−**3g** have a good solubility in common organic solvents, and **3a**−**3g** are soluble in water, whereas the dioxo precursors (**1a**−**1g**) are insoluble in dichloromethane, chloroform, *n*-hexane, methanol, and acetonitrile and are only sparingly soluble in DMF and DMSO. **2a**−**2e** and **3a**−**3g** are stable in solid form. The TGA thermogram of **2b** (Figure S1 in the Supporting Information) revealed that this complex is stable up to 419 °C, whereas **2e**, **3a**, and **3c** showed the first decomposition temperature at 182, 215, and 257 °C, respectively. All of the complexes are stable in CH_2Cl_2, $CHCl_3$, CH_3CN, or CH_3OH for 1 week, although **3a**−**3g** are stable in aqueous solutions for 2 days.

The ^{1}H NMR spectra of **2a**−**2e** show multiplets at δ 7.03−7.57 that are attributed to the phenyl protons of PPh_3 and N∩N ligands. The signals at δ 6.40−6.82 and 7.58−8.93 correspond to aryl protons of the diimine group. The ^{1}H NMR spectra of **3a**−**3g** display a singlet at δ 3.23−3.41, attributable to the dimethyl protons of coordinated DMSO ligands, whereas the diimine aromatic protons appear at δ 7.53−10.06. The ^{13}C{^{1}H} NMR spectra of **2a**−**2e** and **4** in $CDCl_3$ are well resolved except for the Os−*C*≡N resonances; peaks at δ 116.6−158.6 are attributed to the aromatic carbon atoms of PPh_3 (with the exception of **4**) and diimine ligands. For **3a**−**3g**, the ^{13}C{^{1}H} NMR spectra show the dimethyl carbon atoms of the coordinated DMSO ligands at δ ∼46.6, whereas peaks at δ 119.8−162.9 correspond to the carbon atoms from the diimine and cyano ligands. The ^{13}C{^{1}H} NMR spectra of **3e** in the absence and presence of $Zn(NO_3)_2$ in $CDCl_3$/CD_3OD (2:1 v/v) have been recorded. The signals of cyano carbon atoms shifted from δ 131.1 to δ 134.9 upon the addition of Zn^{2+}. A similar change in the *C*≡N chemical shift from 128.3 to 133.5 ppm was also observed by changing the solvent from acetone-d_6 to CD_3OD. The ^{31}P{^{1}H} NMR spectra show a singlet centered at δ 3.63−4.77 for **2a**−**2e** and δ −38.35 for **4**, revealing that the two trans phosphine ligands are chemically equivalent. Upon the addition of $Zn(NO_3)_2$ to **2e** in CD_3CN, the ^{31}P{^{1}H} NMR signal shifted from δ 3.86 (without Zn^{2+}) to δ 4.88.

The IR spectra of **2a**−**2e** reveal two ν(C≡N) stretches of equal intensity at ∼2050 and 2070 cm^{-1}, consistent with the cis coordination geometry of the CN ligands.[38] For **3a**−**3g**, the two ν(C≡N) bands appear at a higher frequency of ∼2060−2075 and 2083−2090 cm^{-1}. This is consistent with DMSO being a better π acceptor than PPh_3. The two ν(C≡N) bands of **4** are at 2025 and 2059 cm^{-1}, as can be expected because PMe_3 is a superior σ donor compared with DMSO and PPh_3. The reaction of **2c** with excess $Zn(NO_3)_2$ in acetonitrile afforded a greenish-yellow solid of [**2c**·$Zn(NO_3)_2$]$_\infty$, and the corresponding IR spectrum shows the ν(C≡N) doublet at 2065 and 2101 cm^{-1}, which are at higher frequencies than those (2053 and 2068 cm^{-1}) for **2c**. This is consistent with the existence of binding between the cyano moieties and electrophilic Zn^{2+} ions.[39] Similar shifts of ν(C≡N) bands have also been observed upon the addition of $Zn(NO_3)_2$ to **2a** (from (2060, 2076) to (2071, 2105) cm^{-1}) and **2e** (from (2055, 2074) to (2063, 2098) cm^{-1}). The shifting of ν(C≡N) bands due to Zn^{2+} coordination was reversible; upon the addition of excess sodium chloride to a methanolic solution of [**2c**·$Zn(NO_3)_2$]$_\infty$, the solution turned from yellow to red, from which **2c** was isolated and characterized by its ν(C≡N) stretching bands.

The positive FAB mass spectrum of [**2e**·$Zn(NO_3)_2$]$_n$ shows peaks at *m*/*z* 1037, 1163, and 1353, corresponding to the $[M + H]^+$, $[M + H + ZnNO_3]^+$, and $[M + H + Zn(NO_3)_2 + ZnNO_3]^+$ ions, respectively. The electrospray ionization mass spectrum of a methanolic solution of **2e** upon addition of 1000 equiv of $Zn(NO_3)_2$ (Figure S2 in the Supporting Information) displayed similar peaks at *m*/*z* 1162.0 $[M + ZnNO_3]^+$ and 1351.7 $[M + Zn(NO_3)_2 + ZnNO_3]^+$, and upon dilution with methanol/H_2O, their intensities gradually diminished, whereas that of the parent $[M + H]^+$ ion at *m*/*z* 1037.1 slowly increased. Similarly, the positive FAB mass spectrum of [**3a**·$Zn(NO_3)_2$]$_n$ displayed $[M + H + Zn(NO_3)_2 + ZnNO_3]^+$ ions at *m*/*z* 1049, whereas the ESI mass spectrum

(37) (a) Sharipov, A. K. *Russ. J. Appl. Chem.* **2003**, *76*, 108−113. (b) Lyavinets, A. S.; Marushchak, N. T. *Russ. J. Gen. Chem.* **2004**, *74*, 885−889.

(38) (a) Schilt, A. A. *Inorg. Chem.* **1964**, *3*, 1323−1325. (b) Spaulding, L.; Reinhardt, B. A.; Orchin, M. *Inorg. Chem.* **1972**, *11*, 2092−2094.

(39) Shriver, D. F. *Struct. Bonding* **1966**, *1*, 32−58.

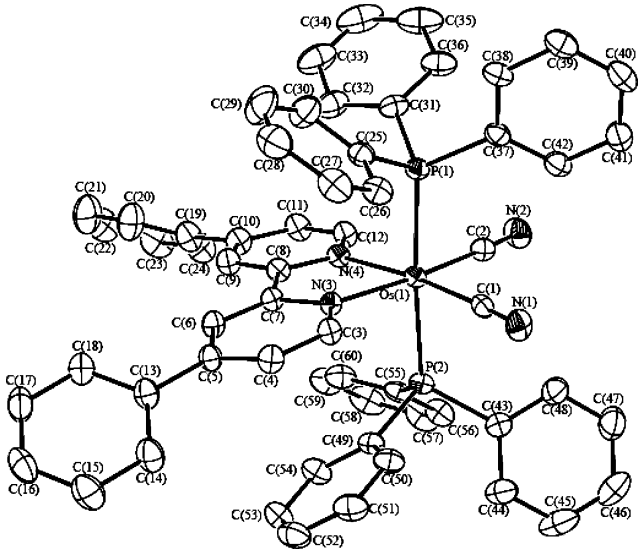

Figure 1. Perspective view of **2d** (30% probability ellipsoids).

in H_2O revealed peaks at *m*/*z* 857.8 $[M + ZnNO_3]^+$ and 1047.7 $[M + Zn(NO_3)_2 + ZnNO_3]^+$.

Crystal Structures. The crystal structures of **2d**, $[\mathbf{2c}\cdot Zn(NO_3)_2]_\infty$, **3b**, and **4** (ORTEP diagrams in Figures 1−4), and **2a**, **2c**, **2e**, **3d**, and **3e** (Figures S3−S7 in the Supporting Information) have been determined; selected bond lengths and angles are listed in Table 2 and Table S2 in the Supporting Information. The two cyano ligands are cis to each other, and the mean Os−C bond lengths of **2a** and **2c**−**2e** are ∼2.02 Å, which are comparable to that in $[OsO_2(CN)_2(pyridine)_2]$ (2.039 Å)[29] and $[OsO_2(CN)_2(Ph_2phen)]$ (2.02 and 2.053 Å).[27] The average cyano C≡N distance is 1.14 Å, which is typical for the unbridged C≡N termini (1.15 Å in $[Fe(CN)_4(CO)_2]^{2-}$ and $[Mn(CN)_3(CO)_3]^{2-}$).[40] The two PPh_3 ligands of **2a** and **2c**−**2e** are trans to each other with a mean Os−P bond length of 2.36 Å, similar to Os−P distances observed in $[Os\{PH(OMe)Ph\}(CO)_2(PPh_3)_2]$ (∼2.34 Å)[41] and *mer*-$[OsCl(SC_6F_5)(N_2)(PMe_2Ph)_3]$ (∼2.38 Å for Os−P distances not residing trans to SC_6F_5).[42] For **2a**, the phenyl substituents of the Ph_2phen ligand are displaced by a mean angle of 54° from the plane of 1,10-phenanthroline (Figure S3 in the Supporting Information). Similarly, for **2d**, the phenyl rings are displaced by ∼36° from the bpy plane (Figure 1). There are intermolecular C≡N···H−$CHCl_2$ hydrogen-bonding interactions (2.689 Å) and short contacts (<3.35 Å) between PPh_3 ligands and CH_3CN solvent molecules.

The X-ray crystal structure of $[\mathbf{2c}\cdot Zn(NO_3)_2]_\infty$ (Figure 2) contains 1D zigzag polymeric chains with alternate $[Os(PPh_3)_2(CN)_2(phen)]$ and $Zn(NO_3)_2$ units. The N−C−Os (172.9(5)°) and C−N−Zn angles (168.5(5)°) are slightly bent from 180°. The structural parameters of the $[Os(PPh_3)_2(CN)_2(phen)]$ units in $[\mathbf{2c}\cdot Zn(NO_3)_2]_\infty$ are comparable to those in **2c** (Figure S4 in the Supporting Information). The two CN ligands are coordinated to $[Zn(NO_3)_2]$, and the coordination sphere around the zinc atoms can be described as a distorted trigonal bipyramid, with one η^2- (bidentate: Zn−O 1.91(1), 2.37(1) Å) and one η^1-nitrate (Zn−O 2.24(1) Å) ion, plus two cyanide groups from $[Os(PPh_3)_2(CN)_2(phen)]$ molecules (Zn−N 1.935(5) Å).

3b (Figure 3) shows a geometry similar to that of the PPh_3 derivatives, **2a** and **2c**−**2e**. The mean Os−C, C≡N, and Os−N bond lengths are 2.02, 1.15, and 2.13 Å respectively, which are comparable to those in **2a** and **2c**−**2e**. The mean Os−S distance of 2.30 Å is comparable to those reported for $[OsX_2(DMSO)_4]$ (2.34−2.35 Å; X = Cl^-, Br^-).[43] Apart from intermolecular interactions between the cyanide ligands and solvent molecules (methanol), there are short intermolecular contacts (2.34−2.65 Å) from the coordinated $O{=}S(CH_3)_2$ ligands to the aromatic C−*H* groups of bipyridine and DMSO hydrogens.

Intermolecular interactions between the cyanide and phen ligands (aryl C−H···N≡C intermolecular contact = 2.587 Å) were observed in the crystal structure of **4** (Figure 4), and water molecules are present between the methyl groups of PMe_3 and cyanide or aryl (C−H) groups of adjacent molecules. The intermolecular C≡N···H_2O, H_2O···H−C(PMe_3), and H_2O···H−C(phen) distances lie in the range of 2.460−2.824 Å.

Absorption and Emission Spectroscopy. The UV−vis absorption data of **2a**−**2e** and **4** in CH_2Cl_2, and those of **3a**−**3g** in CH_2Cl_2 and H_2O are listed in Table 3; the spectral data measured in other solvents are given in the Supporting Information (Table S3). All of the complexes are soluble in common organic solvents with the exception of **2b**, which is sparingly soluble in dichloromethane, chloroform, and methanol. **2a**−**2e** display an intense absorption band with λ_{max} at 269−313 nm (ϵ = (2.50−4.55) × 10^4 M^{-1} cm^{-1}), together with a broad and moderately intense absorption at λ_{max} 406−446 nm (ϵ = (3.10−10.0) × 10^3 M^{-1} cm^{-1}) and tailing to 520−580 nm (ϵ = (600−1800) M^{-1} cm^{-1}) in CH_2Cl_2 solutions. In the literature, $[Ru(bpy)_3]^{2+}$ and $[Os(bpy)_3]^{2+}$ have individually been reported to display an intense low-energy absorption band with λ_{max} at 450 and 480 nm, respectively, both of which have been assigned to MLCT transitions.[44] Thus, the low-energy absorptions of **2a**−**2e** at 406−446 nm are assigned to ^{1}MLCT: $(d_\pi)Os \rightarrow \pi^*(N^\frown N)$ transitions, whereas the tailings at 520−580 nm with ϵ values of (600−1800) M^{-1} cm^{-1} could be due to ^{3}MLCT transitions.

The solvent effect on the absorption spectra of **2a**−**2e** has been investigated, and the data are given in the Supporting Information (Table S3). For **2e**, the high-energy absorption

(40) Contakes, S. M.; Hsu, S. C. N.; Rauchfuss, T. B.; Wilson, S. R. *Inorg. Chem.* **2002**, *41*, 1670−1678.
(41) Bohle, D. S.; Jones, T. C.; Rickard, C. E. F.; Roper, W. R. *J. Chem. Soc., Chem. Commun.* **1984**, 865−867.
(42) Cruz-Garritz, D.; Gelover, S.; Torrens, H.; Leal, J.; Richards, R. L. *J. Chem. Soc., Dalton Trans.* **1988**, 2393−2396.
(43) (a) Robinson, P. D.; Hinckley, C. C.; Ikuo, A. *Acta Crystallogr., Sect. C* **1989**, *45*, 1079−1080. (b) McDonagh, A. M.; Humphrey, M. G.; Hockless, D. C. R. *Aust. J. Chem.* **1998**, *51*, 807−811.
(44) (a) Creutz, C.; Chou, M.; Netzel, T. L.; Okumura, M.; Sutin, N. *J. Am. Chem. Soc.* **1980**, *102*, 1309−1319. (b) Pankuch, B. J.; Lacky, D. E.; Crosby, G. A. *J. Phys. Chem.* **1980**, *84*, 2061−2067. (c) Ferguson, J.; Herren, F.; Krausz, E. R.; Maeder, M.; Vrbancich, J. *Coord. Chem. Rev.* **1985**, *64*, 21−39. (d) Meyer, T. J. *Pure Appl. Chem.* **1986**, *58*, 1193−1206. (e) Johnson, S. R.; Westmoreland, T. D.; Caspar, J. V.; Barqawi, K. R.; Meyer, T. J. *Inorg. Chem.* **1988**, *27*, 3195−3200.

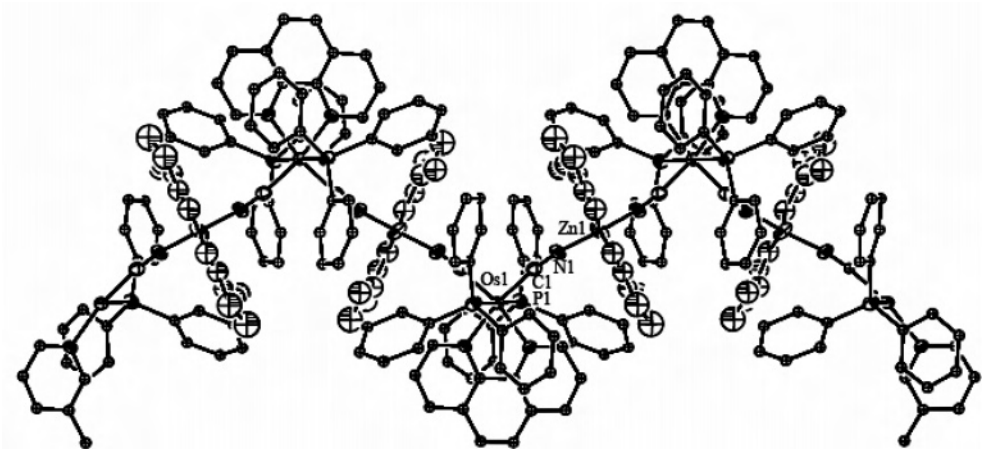

Figure 2. Perspective view of $[\mathbf{2c}\cdot Zn(NO_3)_2]_\infty$ (30% probability ellipsoids).

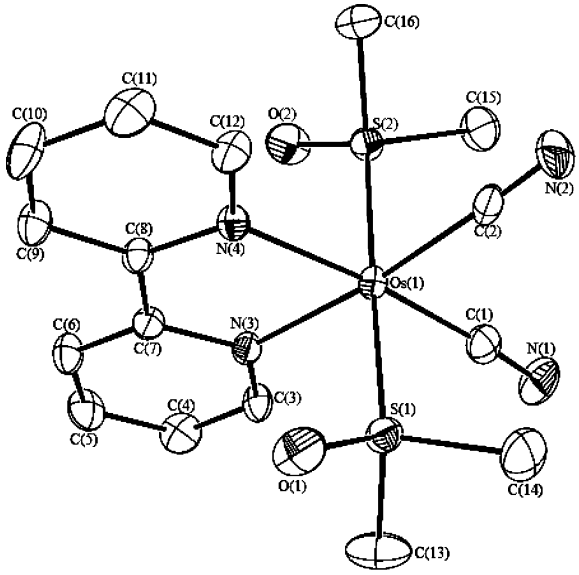

Figure 3. Perspective view of **3b** (30% probability ellipsoids).

maximum shows a minor shift from λ_{max} at 291 nm (ϵ = 23000 M^{-1} cm^{-1}) in CH_3OH to 298 nm (ϵ = 28300 M^{-1} cm^{-1}) in benzene, whereas the low-energy absorption bands at $\lambda > 400$ nm display a substantial solvatochromism: the largest shift of peak maximum is from 410 nm (ϵ = 3130 M^{-1} cm^{-1}) in CH_3OH to 460 nm (ϵ = 2500 M^{-1} cm^{-1}) in toluene ($\Delta\nu$ = 2650 cm^{-1}). The electronic absorption spectra of **2e** in different solvents at 298 K are depicted in part a of Figure 5, and a plot of the absorption energies for **2e** versus the solvent polarity, as defined by the E_T value (classified with respect to the longest-wavelength solvatochromic absorption band of the pyridinium *N*-phenolate betaine dye),[45] affords a linear correlation, as shown in part b of Figure 5. The absorption bands of **2a**, **2c**, and **2d** at 387−440 nm show similar solvatochromism, and the maximum shift in λ_{max} values are 750 cm^{-1} for **2d**, 1570 cm^{-1} for **2c**, and 2290 cm^{-1} for **2a** when the solvent changes from methanol to THF or toluene. The molar extinction coefficient for **2c** changes markedly from ϵ = 3200 M^{-1} cm^{-1} at 408 nm in pyridine to 6700 M^{-1} cm^{-1} at 398 nm in DMSO. **4** shows the absorption peak maximum varying from 404 nm in methanol to 465 nm in chloroform (Figure S9 in the Supporting Information).

Upon excitation at 420 nm, **2a**−**2e** show an intense emission with λ_{max} at 602−717 nm. The effect of solvents on the emission properties has been examined. As an example, the emission λ_{max} of **2e** (concentration = 3×10^{-5} M) varies with the solvent (Table S3 in the Supporting Information and Figure 6) from 627 nm in CH_3OH to 707 nm in toluene ($\Delta\nu_{max}$ = 1800 cm^{-1}); the emission quantum yield (Φ) and lifetime (τ) decrease for lower emission energies. The maximum Φ and τ values of **2e** occur in CH_3OH (0.035 and 0.31 μs respectively (λ_{max} = 627 nm)), and these values decrease to 0.017 and 0.19 μs in DMF (λ_{max} = 662 nm), and 0.003 and 0.09 μs in toluene (λ_{max} = 707 nm). The long emission lifetime in the microsecond regime suggests triplet parentage for the emissive excited state.

For **2a**, its emission λ_{max} shows a similar bathochromic shift from 637 nm in methanol to 712 nm in toluene. The absorption (λ_{abs} = 398−438 nm) and emission (λ_{em} = 637−712 nm) maxima of **2a** in various solvents are red-shifted from those of λ_{abs} = 387−412 nm and λ_{em} = 621−661 nm observed for **2c**. Because of its poor solubility, the photophysical properties of **2b** can only be examined in methanol, dichloromethane, and chloroform. **2d** has a better solubility than **2b**, and its photophysical properties in different solvents have been examined. The solvent effect on the emission λ_{max} for **2d** is also evident, where λ_{max} varies from 650 nm in methanol to 717 nm in THF.

The solid-state emission of **2e** at 298 K exhibits a structureless band with λ_{max} at 670 nm (τ = 0.15 μs), which blue-shifts to 632 nm with a lifetime of 1.06 μs at 77 K. In a 77 K glassy MeOH/EtOH (1:4) solution, the emission λ_{max} blue-shifts to 560 nm (τ = 16.1 μs). Similarly, the solid-state emission of **2b** exhibits a broad band at λ_{max} 622 nm with a quantum yield of 0.017 at room temperature. Compared with the PPh_3 counterpart (**2c**), the emissions λ_{max} of **4** are red-shifted and have lower quantum yields and shorter lifetimes both in the solid state and in solutions. Solvatochromism has also been observed for the emission

(45) (a) Dimroth, K.; Reichardt, C.; Siepmann, T.; Bohlmann, F. *Justus Liebigs Ann. Chem.* **1963**, *661*, 1−37. (b) Marcus, Y. *Chem. Soc. Rev.* **1993**, *22*, 409−416.

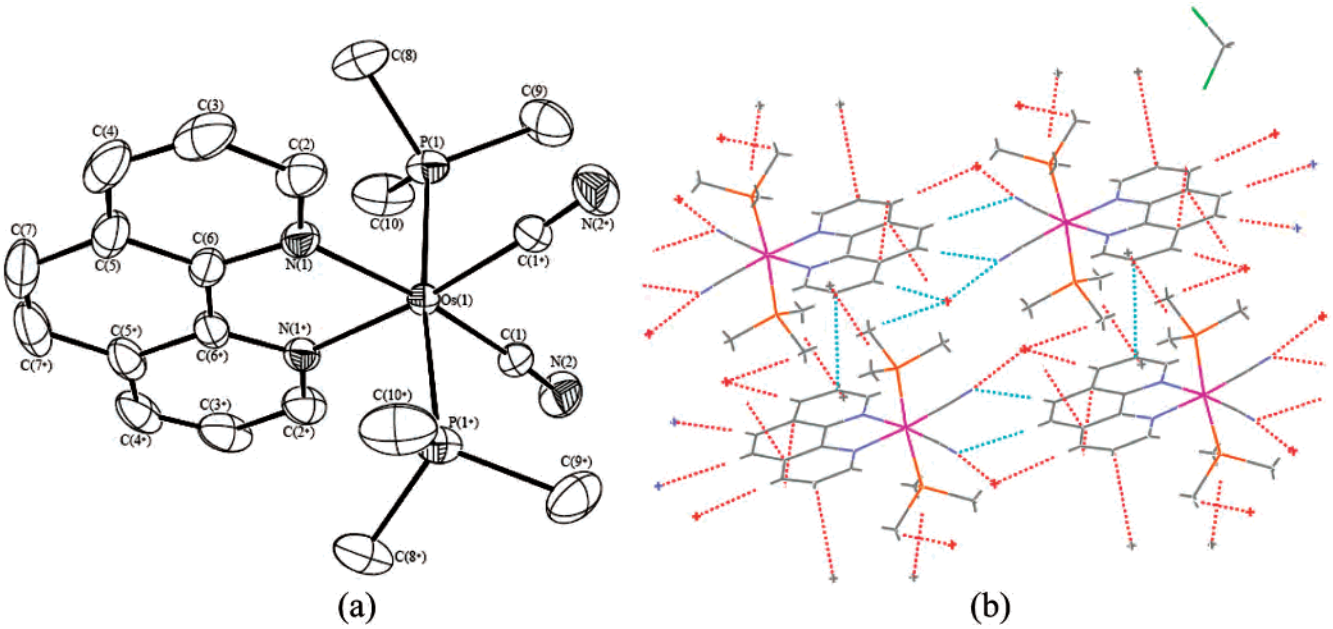

Figure 4. (a) Perspective view of **4** (30% probability ellipsoids). (b) Crystal packing diagram.

Table 2. Selected Bond Lengths (Angstroms) and Angles (Degrees)

	$[\mathbf{2c}\cdot Zn(NO_3)_2]_\infty$		
Os(1)−C(1)	1.993(6)	Zn(1)−N(1)	1.935(5)
N(1)−C(1)	1.140(6)	Zn(1)−O(1)	1.91(1)
Os(1)−N(2)	2.124(4)	Zn(1)−O(2)	2.37(1)
Os(1)−P(1)	2.381(1)	Zn(1)−O(4)	2.24(1)
C(1)−Os(1)−C(1*)	97.9(3)	N(1)−C(1)−Os(1)	172.9(5)
C(1)−Os(1)−N(2)	169.7(2)	C(1)−N(1)−Zn(1)	168.5(5)
C(1*)−Os(1)−N(2)	92.3(2)	N(1*)−Zn(1)−N(1)	123.5(3)
N(2)−Os(1)−N(2*)	77.4(2)	O(4)−Zn(1)−O(2)	134.9(6)
P(1)−Os(1)−P(1*)	178.81(7)	O(1)−Zn(1)−O(4)	75.1(7)
C(1)−Os(1)−P(1)	89.4(2)	N(1)−Zn(1)−O(4)	109.8(3)
N(2*)−Os(1)−P(1*)	90.2(1)	O(1)−Zn(1)−N(1)	112.3(4)
	$\mathbf{2d}\cdot CH_2Cl_2\cdot CH_3CN$		
Os(1)−C(1)	2.030(4)	Os(1)−N(3)	2.109(3)
Os(1)−C(2)	2.022(4)	Os(1)−N(4)	2.118(3)
N(1)−C(1)	1.145(5)	Os(1)−P(1)	2.361(1)
N(2)−C(2)	1.149(6)	Os(1)−P(2)	2.387(1)
C(1)−Os(1)−C(2)	94.2(2)	P(1)−Os(1)−P(2)	175.45(3)
C(1)−Os(1)−N(3)	94.4(1)	C(1)−Os(1)−P(2)	86.7(1)
C(2)−Os(1)−N(3)	171.5(1)	N(3)−Os(1)−P(2)	89.83(9)
N(3)−Os(1)−N(4)	76.7(1)	N(1)−C(1)−Os(1)	175.3(4)
	$\mathbf{3b}\cdot CH_3OH$		
Os(1)−C(1)	2.019(8)	Os(1)−N(3)	2.131(5)
Os(1)−C(2)	2.014(7)	Os(1)−S(1)	2.303(2)
N(1)−C(1)	1.141(9)	Os(1)−S(2)	2.305(2)
N(2)−C(2)	1.150(9)	S(1)−O(1)	1.468(5)
C(1)−Os(1)−C(2)	90.7(3)	S(1)−Os(1)−S(2)	178.69(6)
C(1)−Os(1)−N(3)	96.1(2)	C(1)−Os(1)−S(1)	88.9(2)
C(1)−Os(1)−N(4)	173.1(2)	N(3)−Os(1)−S(1)	90.9(2)
N(3)−Os(1)−N(4)	77.0(2)	N(1)−C(1)−Os(1)	176.2(7)
	$\mathbf{4}\cdot CH_2Cl_2\cdot 2H_2O$		
Os(1)−C(1)	1.989(4)	Os(1)−N(1)	2.105(3)
N(2)−C(1)	1.169(6)	Os(1)−P(1)	2.345(1)
C(1)−Os(1)−C(1*)	95.1(2)	P(1)−Os(1)−P(1*)	173.78(6)
C(1)−Os(1)−N(1*)	93.4(2)	C(1)−Os(1)−P(1)	86.8(1)
C(1)−Os(1)−N(1)	171.5(1)	N(1)−Os(1)−P(1)	93.11(9)
N(1)−Os(1)−N(1*)	78.2(2)	N(2)−C(1)−Os(1)	174.5(4)

of **4**; its emission λ_{max} varies from 701 nm in methanol with a τ of 0.092 μs to 760 nm in ethyl acetate with a τ of 0.033 μs.

In nonaqueous solutions, the absorption λ_{max} of **3a**−**3e** (332−390 nm) are blue-shifted from those of the **2a**−**2e** counterparts (387−460 nm). The emission λ_{max} of **3a**−**3e** (583−640 nm) are at higher energies than those of **2a**−**2e** at 621−717 nm. The absorption and emission properties of **3a**−**3e** are solvent-dependent. For **3b**, its absorption λ_{max} varies from 341 nm in H_2O to 376 nm in CH_2Cl_2, and its emission λ_{max} red-shifts from 563 nm in H_2O to 630 nm in DMF. The emission quantum yield and lifetime of **3e** vary from 0.03 and 0.22 μs in H_2O to 0.27 and 0.96 μs in $CHCl_3$, respectively. The absorption and emission properties of **3a**−**3e** have been examined in aqueous solutions. As an example, the UV−vis absorption and emission spectra of **3b** in aqueous solution are depicted in Figure 7. The excitation spectrum of **3b** in H_2O, monitored at emission λ_{max} 563 nm, shows peak maxima at 296, 331, and 376 nm, which matches the ground-state absorption spectrum. The room-temperature solid-state emission of **3b** shows a broad band at λ_{max} 581 nm with a quantum yield of 0.37, the latter being significantly higher than that of 0.017 for the PPh_3 congener, **2b**. For **3f** and **3g** containing the Br_2phen and Clphen ligands, respectively, their absorption λ_{max} at 376 and 363 nm are red-shifted from that of **3c** at 352 nm in CH_2Cl_2 solution. Similarly, the emissions λ_{max} of **3f** and **3g** at 626 and 615 nm respectively are red-shifted from that of **3c** at λ_{max} 600 nm in CH_2Cl_2 solution.

Because the emission energy of the *cis*-dicyanoosmium(II) complexes are solvent-dependent, it is pertinent to apply the energy-gap law to this system.[46] Figure 8 shows a plot of ln k_{nr} against the ^{3}MLCT emission energy of **2c** at 298 K in various solvents. There is a linear decrease in ln k_{nr} with increasing energy gap (E_{em}/cm^{-1}) between the ground and excited states. The slope (−5.02 eV^{-1}) and intercept (24 ± 1) of the plot for **2c** were obtained, and comparisons were made with the values of ca. −7.5 eV^{-1} and 28−30,

(46) (a) Caspar, J. V.; Kober, E. M.; Sullivan, B. P.; Meyer, T. J. *J. Am. Chem. Soc.* **1982**, *104*, 630−632. (b) Caspar, J. V.; Meyer, T. J. *J. Phys. Chem.* **1983**, *87*, 952−957.

Table 3. Photophysical Data of **2a**−**2e**, **3a**−**3g**, and **4**

complex	medium (T/K)	λ_{abs}[a]/nm (ϵ / $M^{-1}cm^{-1}$)	λ_{em}[b] / nm; τ/μs	Φ_{em}
2a	CH_2Cl_2 (298)	284 (45 500), 323 (sh, 11 800), **416** (10 000), 447 (sh, 8500), 521 (sh, 1800)	667; 0.67	0.063
	solid (298)		707; 0.39	
	solid (77)		675; 2.66	
	glass[c] (77)		582; 15.9	
2b	CH_2Cl_2 (298)	296 (24 800), 328 (sh, 6300), **446** (3100), 555 (sh, 640)	665; 0.16	0.012
	solid (298)		622; 0.21	0.017
	solid (77)		602; 3.06	
	glass[c] (77)		575; 14.4	
2c	CH_2Cl_2 (298)	269 (33 300), 295 (sh, 18 600), **406** (6300), 430 (sh, 5900), 525 (sh, 1100)	654; 0.53	0.046
	solid (298)		622; 0.18	
	solid (77)		605; 2.85	
	glass[c] (77)		562; 25.1	
2d	CH_2Cl_2 (298)	313 (37 500), 348 (15 200), **431** (8800), 462 (sh, 8300), 580 (sh, 1400)	703; 0.16	0.010
	solid (298)		663; <0.1	
	solid (77)		646; 0.57	
	glass[c] (77)		585; 18.5	
2e	CH_2Cl_2 (298)	295 (28 400), **440** (3700), 550 (sh, 620)	657; 0.27	0.022
	solid (298)		670; 0.15	
	solid (77)		632; 1.06	
	glass[c] (77)		560; 16.1	
3a	CH_2Cl_2 (298)	271 (32 500), 291 (31 400), 313 (sh, 11 300), **361** (10 900), 406 (sh, 7020), 471 (sh, 1390)	609; 1.42	0.34
	H_2O (298)	288 (38 500), **328** (sh, 15 000), 380 (sh, 8500)	563; 1.22	0.15
	solid (298)		610; 0.18	
	solid (77)		578, 611; 1.58, 1.65	
	glass[c] (77)		540; 12.4	
3b	CH_2Cl_2 (298)	280 (18 300), 307 (sh, 6200), 316 (sh, 5000), **376** (3500), 393 (sh, 3100), 487 (sh, 520)	613; 0.45	0.070
	H_2O (298)	266 (23 000), 304 (14 600), 315 (13 900), **341** (5000), 411 (sh, 850)	563; 0.33	0.085
	solid (298)		581; 0.47	0.37
	solid (77)		560; 4.67	
	glass[c] (77)		532; 11.2	
3c	CH_2Cl_2 (298)	260 (28 200), 274 (sh, 16 200), 290 (sh, 11 800), **352** (5320), 391 (sh, 4160), 462 (sh, 660)	600; 1.20	0.22
	H_2O (298)	272 (24 500), 316 (sh, 6380), 348 (sh, 4480), **365** (4040), 409 (sh, 940)	553; 0.40	0.068
	solid (298)		573; 0.45	
	solid (77)		552, 556; 7.20, 7.77	
	glass[c] (77)		524, 550 (sh); 16.8	
3d	CH_2Cl_2 (298)	258 (27 800), 298 (41 600), 323 (sh, 16 600), **386** (8910), 401 (sh, 8250), 498 (sh, 1210)	623; 0.55	0.13
	H_2O (298)	286 (24 500), 323 (sh, 10 700), **357** (5780)	574; 0.45	0.085
	solid (298)		622; 0.15	
	solid (77)		561, 606; 0.44, 0.56	
	glass[c] (77)		543; 13.5	
3e	CH_2Cl_2 (298)	255 (sh, 8400), 279 (15 500), 303 (sh, 6200), 313 (sh, 5200), **370** (3100), 464 (sh, 500)	598; 0.78	0.16
	H_2O (298)	255 (sh, 16 600), 270 (19 200), 302 (11 500), 312 (10 800), **340** (4500), 402 (sh, 1000)	555; 0.22	0.030
	solid (298)		589; 0.30	
	solid (77)		555; 3.86	
	glass[c] (77)		530; 10.6	
3f	CH_2Cl_2 (298)	269 (22 900), 286 (sh, 14 000), 313 (sh, 4600), **376** (4200), 403 (sh, 3500), 488 (sh, 850)	626; 0.61	0.10
	H_2O (298)	283 (26 000), 326 (sh, 7300), **360** (4300), 377 (sh, 3800)	579; 0.53	0.14
	solid (298)		630; 0.11	
	solid (77)		611; 1.04	
	glass[c] (77)		552; 9.37	
3g	CH_2Cl_2 (298)	264 (21 000), 279 (sh, 11 300), 288 (sh, 8800), **363** (3700), 399 (sh, 3000), 484 (sh, 740)	615; 0.87	0.19
	H_2O (298)	277 (23 600), 318 (sh, 7100), **355** (4000), 372 (sh, 3300), 412 (sh, 870)	567; 0.69	0.22
	solid (298)		609; 0.42	
	solid (77)		590; 4.15	
	glass[c] (77)		551; 11.1	
4	CH_2Cl_2 (298)	266 (38 100), 289 (sh, 11 100), 314 (sh, 2570), 435 (6400), **459** (6490), 558 (sh, 1190)	728; 0.072	0.0017
	solid (298)		678, 707 (max); 0.15	
	solid (77)		660; 2.41	
	glass[c] (77)		612; 11.7	

[a] The bold number indicates λ_{max} for the MLCT absorption band. [b] Excitation wavelength at 420 nm for **2a**−**2e** and **4**, and 370 nm for **3a**−**3g**. [c] Measured in MeOH/EtOH = 1:4.

respectively, for the $[OsX_4L]$ and $[OsX_2L_2]$ series (X = halides, nitrogen donors, phosphines, or CO; L = bpy or phen).[47] Similarly, a plot of ln k_{nr} versus E_{em} for **3e** in aprotic solvents afforded a straight line with slope of -9.84 eV^{-1} and an intercept of 34 ± 2, and the data are given as Supporting Information (Figure S10). The emission spectrum of **3c** in H_2O recorded 0.2 ps after laser excitation at 266 nm shows a broad band with λ_{max} ~470 nm, which undergoes a single-exponential decay with a rate constant k of ~2×10^{12} s^{-1} to the ^{3}MLCT excited state. *We assign the 470 nm emission to originate from the ^{1}MLCT excited state.*

Effects of Metal Ions upon Photoluminescence. (I) In Acetonitrile or Methanol Solution. Because the emission energies of **2a**−**2e** and **3a**−**3g** are solvent-sensitive, we have

(47) (a) Caspar, J. V.; Meyer, T. J. *J. Am. Chem. Soc.* **1983**, *105*, 5583−5590. (b) Kober, E. M.; Caspar, J. V.; Lumpkin, R. S.; Meyer, T. J. *J. Phys. Chem.* **1986**, *90*, 3722−3734.

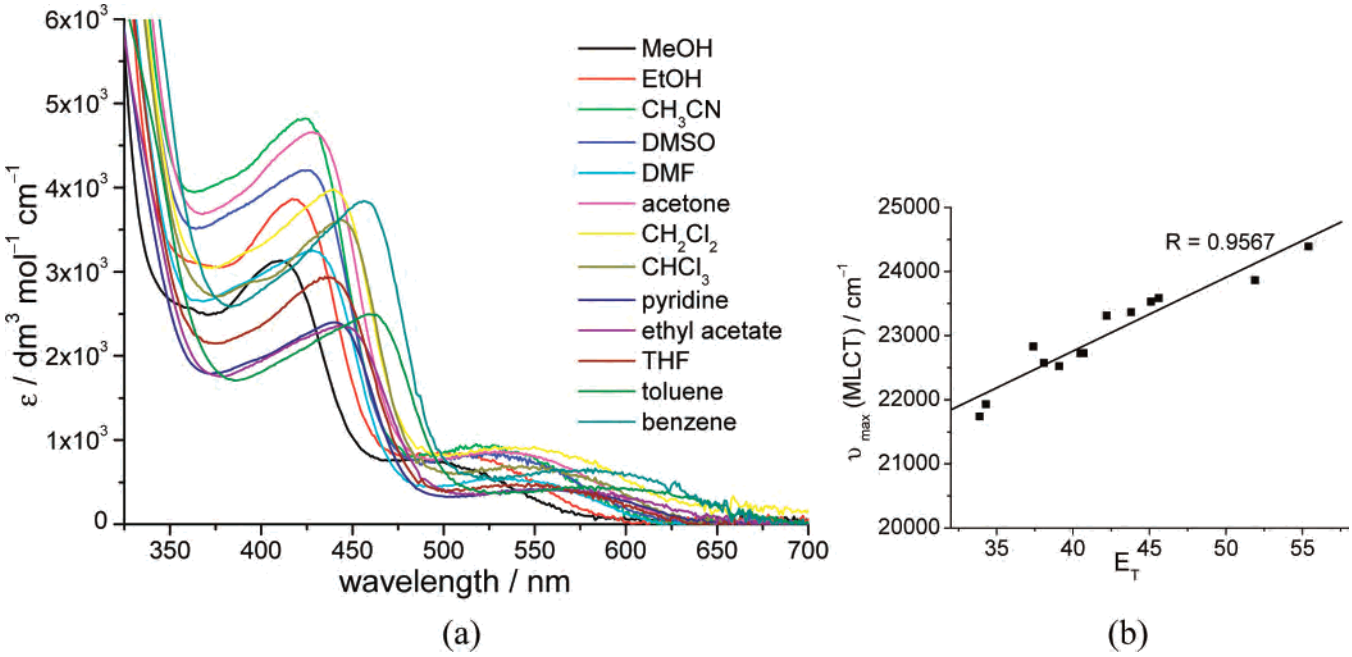

Figure 5. (a) UV−vis absorption spectra of **2e** in various solvents at 298 K. (b) Plot of absorption energies in cm^{-1} for **2e** against E_T value of solvents.

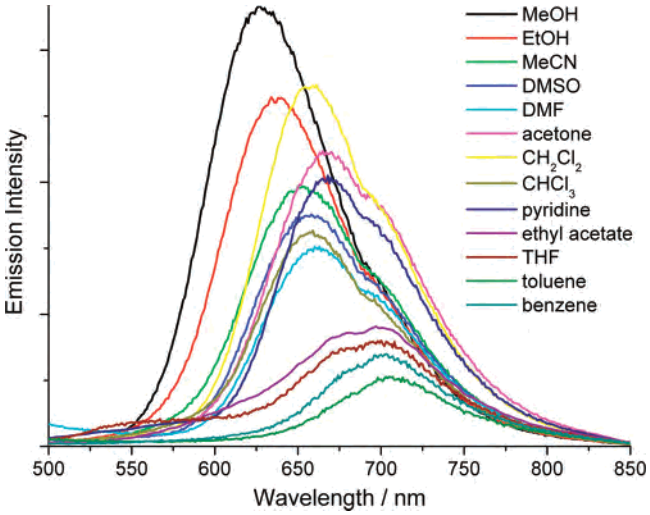

Figure 6. Emission spectra of **2e** in various solvents at 298 K.

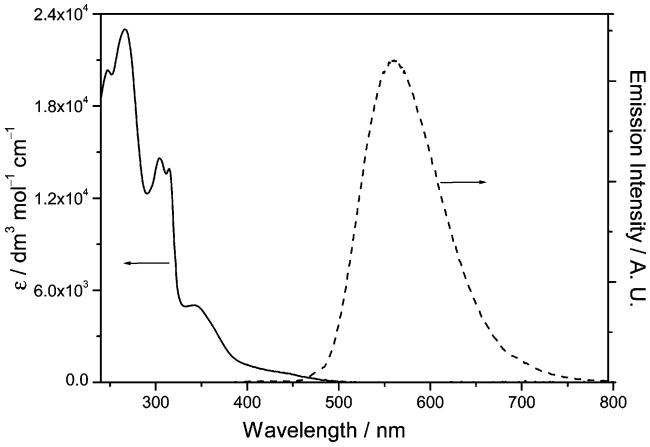

Figure 7. Absorption (solid) and emission (dash, λ_{ex} = 370 nm) spectra of **3b** in H_2O at 298 K.

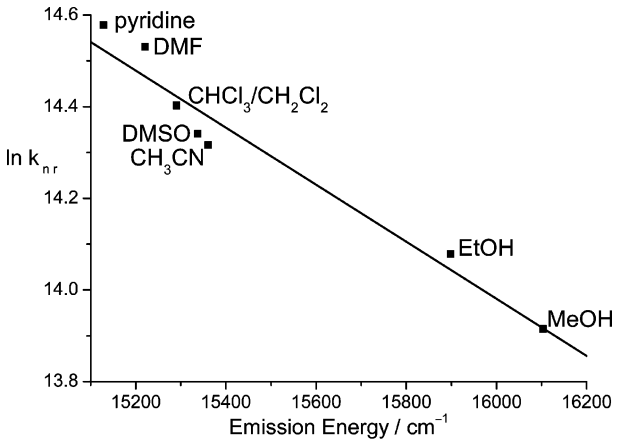

Figure 8. Plot of ln k_{nr} against E_{em} for **2c** in various solvents at 298 K.

also examined the absorption and emission properties of this class of complexes in the presence of metal ions (M^{n+}). For **2e**, upon the addition of up to 2 equiv of $Zn(NO_3)_2$, the absorption λ_{max} gradually shifted from 424 to 367 nm and the weak low-energy band at 526 nm diminished. When more than 2 equiv of Zn^{2+} ions were added, a slight further red-shift of the absorption maximum from 367 to 371 nm (with 10 equiv of Zn^{2+}) was recorded. The absorption spectral traces are not isosbestic, and the data are provided in the Supporting Information.

The emission spectral traces of **2e** in a 0.1 M $^nBu_4NPF_6$ methanolic solution upon the addition of $Zn(NO_3)_2$ in methanol at different concentrations were recorded (Figure 9). A plot of the emission intensity enhancement factor (I/I_o) at 531 nm versus the number of equivalents of Zn^{2+} is given in the inset of Figure 9. Upon the addition of up to 2 equiv of $Zn(NO_3)_2$, the emission λ_{max} significantly blue-shifts to 531 nm, with concomitant enhancement of the I/I_o value (up to 810 at λ = 531 nm) and emission lifetime (from 0.31 to 2.4 μs). Further addition of $Zn(NO_3)_2$ led to a slight decrease in the emission intensity and a red-shift in the emission λ_{max} to 541 nm (at 10 equiv of Zn^{2+}). When

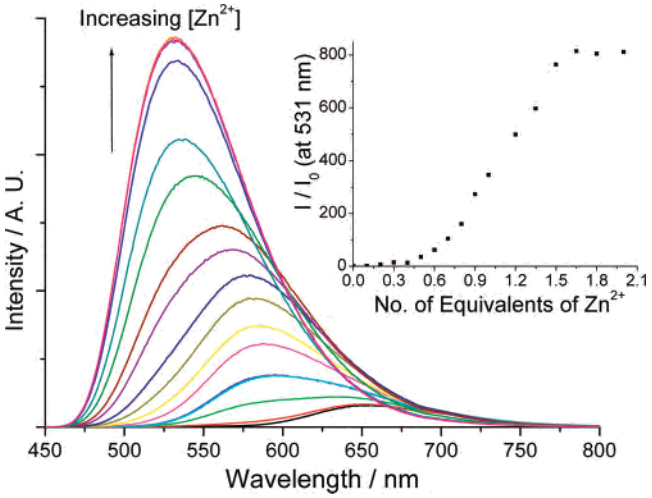

Figure 9. Emission spectral traces and (inset) emission intensity enhancement factor (I/I_o, monitored at 531 nm) of **2e** at increasing equivalents of $Zn(NO_3)_2$ in 0.1 M $^nBu_4NPF_6$ methanolic solution at 298 K ($\lambda_{ex} = 420$ nm, [**2e**] $= 4.96 \times 10^{-5}$ M).

monitoring at 541 nm, the excitation spectrum of **2e** in the presence of 10 equiv of $Zn(NO_3)_2$ is similar to that of the ground-state absorption spectrum under the same conditions.

The effect of other cations has also been investigated. Addition of 2 equiv of $Cu(ClO_4)_2$ to a 0.1 M $^nBu_4NPF_6$ acetonitrile solution of **2c** led to a blue-shift of the absorption maximum from 397 to 342 nm and complete quenching of the emission. The presence of 100 equiv of $LiClO_4$ or $NaClO_4$ did not cause a dramatic change in the emission properties; the emission intensity only decreased by ~50 and 10%, and the emission λ_{max} slightly shifted to 645 and 650 nm, respectively. Blue shifts in emission λ_{max} ($\Delta\nu_{max} = 3460$ cm^{-1}) and I/I_o values of 200−1500 were also observed upon addition of 200 equiv of $Mg(ClO_4)_2$, $Cd(ClO_4)_2$, or $Zn(ClO_4)_2$ to **2c** in 0.1 M $^nBu_4NPF_6$ acetonitrile solution. Similar findings on the changes in the emission properties of **3a**−**3e** in acetonitrile solutions upon the addition of $Zn(NO_3)_2$ were also recorded. As an example, the emission of **3a** in 0.1 M $^nBu_4NPF_6$ acetonitrile solution shows a blue shift in λ_{max} from 626 to 540 nm and I/I_o of 124 at 540 nm upon the addition of up to 2 equiv of $Zn(NO_3)_2$.

(II) In Aqueous Solution. The addition of up to 10 equiv of $Zn(NO_3)_2$ to an aqueous solution of **3a** at 298 K did not cause a notable blue-shift in emission λ_{max} or a substantial enhancement of emission intensity (maximum $I/I_o = 1.5$ at 562 nm with 2 equiv of Zn^{2+}). This reveals that the binding of Zn^{2+} to **3a** is significantly diminished in aqueous medium. Emission titration of **3a** upon the addition of different concentrations of $Zn(NO_3)_2$ in 0.1 M $^nBu_4NPF_6$ aqueous solution was undertaken; addition of Zn^{2+} (up to 3 equiv) induced no shift in the emission λ_{max} at 563 nm. The emission intensity at λ_{max} was slightly affected by the addition of $Zn(NO_3)_2$, but the changes were sporadic and irregular.

Cytotoxicity. The cytotoxicity of **3c** toward a panel of several selected human cancer cell lines (human hepatocellular carcinoma (HepG2), human nasopharyngeal carcinoma (SUNE1), and human breast cancer cells (MCF7)) has been evaluated by the 3-(4,5-dimethylthiazol-2-yl)-2,5-diphenyltetrazolium bromide (MTT) assay.[48] Complex **3c** showed no significant cytotoxicity toward HepG2 and SUNE1 cells, with more than 90% cell survival at a complex concentration up to 50 μM and IC_{50} (inhibitory concentration) values greater than 100 μM.

Electrochemistry. The cyclic voltammograms of **2c**, **3c**, **3f**, **3g**, and **4** in CH_3CN solutions at 298 K were recorded at a scan rate of 100 mV/s using 0.1 M $^nBu_4NPF_6$ as a supporting electrolyte. Complexes **2c**, **3c**, and **4** display one reversible couple at $E_{1/2} = +0.53$, $+0.92$, and $+0.31$ V, respectively. There is also a reversible one-electron reduction couple at $E_{1/2} = -1.97$, -1.70, and -1.93 V for **2c**, **3c**, and **4**, respectively. We assign the couples at $E_{1/2} = +0.31$ to $+0.92$ V to the metal-centered oxidation [Os(III) + $e^- \rightarrow$ Os(II)], whereas the reduction couples at $E_{1/2} = -1.70$ to -1.97 V are due to the reduction of diimine ligands.[49] The $E_{1/2}$ ($Os^{III/II}$) of **3c** at $+0.92$ V is cathodically shifted from that of $+0.53$ V for **2c**, which is consistent with the fact that DMSO is a better π acceptor than PPh_3. The $E_{1/2}$ ($Os^{III/II}$) of **4** at $+0.31$ V could be attributed to PMe_3 being a better σ donor than DMSO and PPh_3. The $E_{1/2}$ ($Os^{III/II}$) values of **3f** ($+0.96$ V) and **3g** ($+0.91$ V) are similar, consistent with the metal-centered assignment for the electrochemical oxidation.

The excited-state redox potentials of *cis*-dicyanoosmium(II) diimine complexes can be estimated from the electrochemical and spectroscopic data. The $E_{1/2}$ ($Os^{III/II*}$) values can be expressed by $E_{1/2}$ ($Os^{III/II*}$) = $E_{1/2}$ ($Os^{III/II}$) − E_{0-0} ($Os^{II*/II}$); the E_{0-0} value can be estimated from low-temperature solid-state emission (2.06 eV for **2c**; 2.26 eV for **3c**; 1.89 eV for **4**), and the $E_{1/2}$ ($Os^{III/II}$) value is obtained from cyclic voltammetric data. Therefore, the $E_{1/2}$ ($Os^{III/II*}$) were calculated to be -1.53, -1.34, and -1.58 V for **2c**, **3c**, and **4** respectively, revealing that the ^{3}MLCT excited states are strong reductants.[50]

Discussion

This work demonstrates that photolysis of $[OsO_2(CN)_2(N^{\frown}N)]$ in the presence of PPh_3, PMe_3, or DMSO is a useful method for the preparation of strongly luminescent *cis*-dicyanoosmium(II) complexes bearing diimine ($N^{\frown}N$) ligands. As dimethyl sulfone was detected after photolysis of $[OsO_2(CN)_2(N^{\frown}N)]$ in DMSO solutions, the photoreduction of dioxoosmium(VI) to osmium(II) likely involves the transfer of an oxygen atom from the electronic excited state(s) of $[OsO_2(CN)_2(N^{\frown}N)]$ to DMSO. The photochemical reactions of $[OsO_2(CN)_2(N^{\frown}N)]$ with PR_3 and DMSO are depicted in Scheme 1. Previous studies showed that *trans*-

(48) Mosmann, T. *J. Immunol. Methods* **1983**, *65*, 55−63.
(49) (a) Collison, D.; Mabbs, F. E.; McInnes, E. J. L.; Taylor, K. J.; Welch, A. J.; Yellowlees, L. J. *J. Chem. Soc., Dalton Trans.* **1996**, 329−334. (b) Chan, S.-C.; Chan, M. C. W.; Wang, Y.; Che, C.-M.; Cheung, K.-K.; Zhu, N. *Chem.—Eur. J.* **2001**, *7*, 4180−4190.
(50) (a) Kober, E. M.; Marshall, J. L.; Dressick, W. J.; Sullivan, B. P.; Caspar, J. V.; Meyer, T. J. *Inorg. Chem.* **1985**, *24*, 2755−2763. (b) Kober, E. M.; Sullivan, B. P.; Dressick, W. J.; Caspar, J. V.; Meyer, T. J. *J. Am. Chem. Soc.* **1980**, *102*, 7383−7385. (c) Kober, E. M.; Caspar, J. V.; Sullivan, B. P.; Meyer, T. J. *Inorg. Chem.* **1988**, *27*, 4587−4598.

dioxoosmium(VI) complexes supported by nitrogen donor and/or CN ligands have a long-lived and emissive $^3[(d_{xy})^1 (d_{xz}, d_{yz})^1]$ excited state in solution and are powerful photooxidants. Indeed, light-induced photochemical oxidation of alkenes to epoxides by $[OsO_2(CN)_2(^tBu_2bpy)]$ complexes had previously been demonstrated.[29] The $[OsO_2(CN)_2(N^{\cap}N)]$ complexes in this work have a long-lived emission in the visible region. As an example, **1e** shows an emission at 653 nm with a lifetime of 0.65 μs and a quantum yield of 6.3×10^{-4} in CH_3CN solution. The emission of **1e** was found to be quenched by DMSO with a quenching rate constant of 3.0×10^9 M^{-1} s^{-1}. This suggests that the photodeoxygenation of **1e** probably occurs via the $^3[(d_{xy})^1 (d_{xz}, d_{yz})^1]$ excited state. This assumption is supported by the finding that the photoreduction of **1e** to **3e** in DMSO occurred efficiently within 30 min upon light excitation at $\lambda = 450$ nm, which is the spectral region for the $d_{xy} \rightarrow (d_{xz}, d_{yz})$ transitions.[28,29,51]

In this work, the ^{3}MLCT emission energy of *cis*-dicyanoosmium(II) complexes are affected by: (1) substituent(s) on the diimine ligand, (2) π-acceptor auxiliary ligands (PR_3 and DMSO), (3) solvent polarity, and (4) the presence of metal cations. Derivatization of the diimine ligand with electron-withdrawing substituents stabilizes the π^* orbital, whereas the electron-donating alkyl substituent increases the energy of the π^* orbital. Thus, the ^{3}MLCT emission energy in acetonitrile decreases in the order: (i) for phen derivatives: **2c** ($\lambda_{em} = 651$ nm) > **2a** (669 nm), whereas **3c** ($\lambda_{em} = 613$ nm) > **3a** (626 nm) > **3g** (628 nm) > **3f** (644 nm), (ii) for bpy derivatives: **2e** ($\lambda_{em} = 653$ nm) > **2b** (656 nm) > **2d** (697 nm), whereas **3e** ($\lambda_{em} = 613$ nm) > **3b** (626 nm) > **3d** (634 nm). The strong π-acceptor axial ligands (L) increase the energy gap between the d_π(Os) and π^* ($N^{\cap}N$) orbitals as a result of d_π(Os) $\rightarrow$ L π backbonding. Because DMSO is a better π acceptor than trimethyl- and triphenylphosphine,[52] the emissions of **3a**−**3g** are at higher energies (λ_{em} = 613−644 nm in CH_3CN) than those observed for **2a**−**2e** (λ_{em} = 651−697 nm) and **4** ($\lambda_{em} = 731$ nm).

In this work, intermolecular interactions between the coordinated cyanide groups and solvent molecules affect the ^{3}MLCT emission of the Os(II) complexes. For example, the emission λ_{max} of **2e** blue-shifts from 707 nm in toluene to 627 nm in CH_3OH. We attribute this to hydrogen-bonding interactions between the protic solvent molecules such as MeOH or EtOH and coordinated CN ligands, which is also revealed by difference in chemical shifts of the cyano carbon atoms of **3e** recorded in CD_3OD and acetone-d_6 (δ 133.5 vs δ 128.3). The cyanide-solvent hydrogen-bonding interaction causes a shift of electron density away from Os(II). As a result, the d_π(Os) level would be lowered, leading to increases in ^{1}MLCT absorption and ^{3}MLCT emission energies in protic solvents.[53] Alternatively, the red-shift of the emission of *cis*-dicyanoosmium(II) diimine complexes in less polar solvents suggests that the dipole moment of the excited-state is lower

Scheme 3

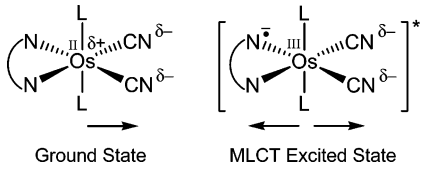

than that of the ground state, and decreasing solvent polarity leads to stabilization of the excited state to a greater degree. This is consistent with the assignment of the emissive excited state to be $d_\pi(Os^{II}) \rightarrow \pi^*(N^{\cap}N)$ in nature, as depicted in Scheme 3.

The solvatochromic behavior of the emission of these Os(II) complexes follows a linear correlation between ln k_{nr} and E_{em}, as predicted by the energy-gap law. A plot of ln k_{nr} against the emission energy of the ^{3}MLCT excited state of **2c** in various solvents afforded a linear correlation with a slope of -5.02 eV^{-1} and an intercept of (24 ± 1), as depicted in Figure 8. A simplified equation for the relationship between ln k_{nr} and the emission energy, E_{em} is: $\ln k_{nr} = (\ln \beta - S_M) - (\gamma_0 E_{em}/\hbar\omega_M)$, assuming a single acceptor vibration.[47a] The β value relates to the spin−orbit coupling constant for osmium(II) complexes. S_M is a measure of excited-state distortion and $\gamma_0 = \ln (E_{em}/S_M \hbar\omega_M) - 1$, where $\hbar\omega_M$ is the vibrational progression of the deactivating mode(s). For **2c** and **3e**, variation in ln β should be small. Well-revolved vibronic low-temperature (77 K) glassy emission spectra of **2c** and **3e** have not been obtained in this work, therefore a quantitative discussion on S_M and γ_0 cannot be made. The slope (-9.84 eV^{-1}) of the plot for **3e** is more negative than that of **2c** (-5.02 eV^{-1}), and the intercept (34 ± 2) for **3e** is relatively larger than that of (24 ± 1) for **2c**, suggesting that the excited-state structural distortion (related to S_M and $\hbar\omega_M$ values) of the former could be smaller than that of the latter. For **3a**−**3f**, the absorption and emission maxima are in general at higher energies than those for **2a**−**2e**. The emission excited states of **3a**−**3f** contain more ^{3}IL character, and, hence, the excited-state distortion of the metal−ligand bond(s) in the case of **3e** could be smaller than that of **2c**, the latter exhibits a ^{3}MLCT excited state. The data for **2c** in protic solvents (MeOH and EtOH) show slight deviations from a linear correlation, and this may be rationalized by hydrogen-bonding interactions between the solvent molecules and cyano groups in the excited state.[19,50a] Similarly, the relatively low Φ and short τ of **3a**−**3e** in aqueous solution can be attributed to hydrogen-bonding contacts between the DMSO ligands and water molecules.

The MLCT absorption and emission maximum of **2e** exhibit hypsochromic shifts upon the addition of metal cations; this shift was also accompanied by an enhancement of the emission intensity. The most-dramatic effect was observed with $Zn(NO_3)_2$: upon the addition of up to 2 equiv of $Zn(NO_3)_2$, the emission λ_{max} in 0.1 M $^nBu_4NPF_6$ in methanol shifted from 627 to 531 nm with a 810-fold increase in I/I_o at λ of 531 nm. Analysis of the solution by ESI mass spectrometry indicated the formation of [**2e**·$Zn(NO_3)_2$·$ZnNO_3$] species. We propose that the cyanide ligands

(51) Miskowski, V. M.; Gray, H. B.; Hopkins, M. D. *Adv. Transit. Met. Coord. Chem.* **1996**, *1*, 159−186.
(52) Cotton, F. A.; Wilkinson, G. In *Advanced Inorganic Chemistry*, 3rd ed.; Wiley & Sons: New York, 1972; p 720.
(53) García Posse, M. E.; Katz, N. E.; Baraldo, L. M.; Polonuer, D. D.; Colombano, C. G.; Olabe, J. A. *Inorg. Chem.* **1995**, *34*, 1830−1835.

of the osmium(II) complexes undergo binding to the electrophilic Zn^{2+} ions, causing a decrease in electron density at Os(II) and leading to destabilization of the ^{3}MLCT excited state and, hence, an increase in the ^{3}MLCT emission energy. The enhancement in emission intensity and blue shift in emission λ_{max} (from 627 to 531 nm) of **2e** in the presence of $Zn(NO_3)_2$ could likely be attributed to a change in the triplet excited state from ^{3}MLCT with λ_{max} at 627 nm to that having mixed ^{3}IL and ^{3}MLCT parentages with λ_{max} at 531 nm. The results of NMR experiments are consistent with the decrease in electron density around Os(II) upon the addition of $Zn(NO_3)_2$. The ^{13}C chemical shift of the cyano carbon atoms of **3e** (δ 131.1 in $CDCl_3/CD_3OD$ (2:1)) and the ^{31}P chemical shift of **2e** (δ 3.86 in CD_3CN) increase to δ 134.9 and δ 4.88, respectively, in the presence of $Zn(NO_3)_2$.

We have determined the crystal structure of [**2c**·$Zn(NO_3)_2]_\infty$ (Figure 2), which comprises $[Zn(NO_3)_2]$ moieties linked via the cyanide groups of **2c** units to form an alternating zigzag chain. The room-temperature solid-state emission of [**2e**·$Zn(NO_3)_2]_\infty$ shows a λ_{max} at 548 nm, which is significantly blue-shifted from that of **2e** (λ_{max} 670 nm). This supports the rationale that the coordination of Zn^{2+} by the CN groups increases the ^{3}MLCT emission energy.

Conclusion

The absorption and emission energies, emission quantum yield, and lifetime of *cis*-dicyanoosmium(II) complexes bearing diimine ligands exhibit remarkable solvatochromism. A linear correlation between MLCT absorption energy and solvent polarity (defined by E_T values) was observed. The energy-gap law was obeyed, as demonstrated by the plot of the nonradiative rate constant against the emission energy. The cyanide ligands are engaged in intermolecular hydrogen-bonding interactions with solvent molecules, causing electron density to shift away from osmium(II) and consequentially higher ^{3}MLCT emission energies. A previous report on the solvatochromic properties of $[Ru(bpy)(CN)_4]^{2-}$ has described the interaction of the externally directed cyanide lone pairs with solvent molecules.[54]

The two cyanide ligands of the *cis*-dicyanoosmium(II) diimine complexes can bind metal ions. The MLCT absorption and emission bands undergo substantial blue shifts in energy, and the emission intensity is significantly enhanced upon complexation of metal ions. The emission enhancement may be a consequence of increased molecular rigidity upon the coordination of Zn^{2+} ions by cyanide groups. The water-soluble Os(II) complexes $[Os(DMSO)_2(CN)_2(N^{\cap}N)]$ (**3a**−**3g**) are potentially applicable in luminescent signaling studies involving molecules of biological interest. Their relatively nontoxic nature, as observed for **3c**, facilitates their future development in biosensory applications. Very recently, we have accomplished the synthesis of the *cis*-dicyanoosmium(II) diimine complex bearing a functionalizable bpy group, $[Os(DMSO)_2(CN)_2(bpy(COOH)_2)]$. Treatment with *N*-hydroxysuccinimide (NHS) is envisaged to give $[Os(DMSO)_2(CN)_2(bpy(NHS)_2)]$, which can readily undergo covalent attachment to biomolecules, and we will publish this work in due course.

Acknowledgment. We are grateful for financial support from the Research Grant Council of the Hong Kong SAR, China (HKU 7030/06P, HKU 7011/07P), The University of Hong Kong (URC-administered Seed Funding Grant 200511159176), and the National Natural Science Foundation of China/Research Grants Council Joint Research Scheme (N_HKU 742/04). We thank Prof. David L. Phillips and Dr. Wai-Ming Kwok for performing time-resolved emission spectroscopy experiments and helpful discussions and the reviewers for their insightful comments.

Supporting Information Available: Characterization data of **2a** and **3a**; crystal data, bond lengths and angles, and perspective view of **2a**·$3CH_2Cl_2$, **2c**·$2CH_2Cl_2$, **2e**·CH_2Cl_2•H_2O, **3d**·$0.5(CH_2Cl_2)$, and **3e**·$0.5(CH_2Cl_2)$·$0.5(Et_2O)$; and selected photophysical spectra. This material is available free of charge via the Internet at http://pubs.acs.org.

IC070290L

(54) Timpson, C. J.; Bignozzi, C. A.; Sullivan, B. P.; Kober, E. M.; Meyer, T. J. *J. Phys. Chem.* **1996**, *100*, 2915−2925.